Biochemistry **2003,** *42,* 8272−8288

Functional and Spectroscopic Characterization of Half-Liganded Iron−Zinc Hybrid Hemoglobin: Evidence for Conformational Plasticity within the T State[†,‡]

Uri Samuni,[§] Laura Juszczak,[§] David Dantsker,[§] Imran Khan,[§] Adam J. Friedman,[§]
José Pérez-González-de-Apodaca,[§] Stefano Bruno,[||] Hilda L. Hui,[⊥] Judith E. Colby,[⊥] Ellen Karasik,[⊥]
Laura D. Kwiatkowski,[⊥] Andrea Mozzarelli,[||] Robert Noble,[⊥] and Joel M. Friedman*[,§]

*Department of Physiology and Biophysics, Albert Einstein College of Medicine, 1300 Morris Park Avenue,
Bronx, New York 10461, Department of Biochemistry and Molecular Biology, University of Parma, Parma, Italy, and
School of Medicine and Biomedical Sciences, State University at Buffalo, and Department of Medicine, University at Buffalo,
Veterans Administration Medical Center, Buffalo, New York 14215*

Received November 8, 2002; Revised Manuscript Received March 24, 2003

ABSTRACT: Functionally distinct conformations of HbA (human adult hemoglobin) were probed using deoxy and diliganded derivatives of symmetric Fe−Zn hybrids of HbA. To expand the range of accessible structures, different environments were utilized including solution, sol−gel encapsulation, and crystals. Further structural and functional modulation was achieved by the addition of allosteric effectors. Functional characterization included oxygen affinity measurements, CO combination rates, and geminate and bimolecular CO recombination, after photodissociation. The conformational properties were studied using visible resonance Raman spectroscopy as a probe of local tertiary structure at the iron-containing hemes and UV resonance Raman spectroscopy as a probe of elements of the globin known to be sensitive to quaternary structure. The combined results show a pattern in which there is a progression of conformational and functional properties that are consistent with a picture in which the T quaternary structure can accommodate a range of tertiary conformations (plasticity). At one end of the distribution is the equilibrium deoxy T state conformation that has the lowest ligand reactivity. At the other end of the distribution are T state conformations with higher ligand reactivity that exhibit "loosened" T state constraints within the globin including the $\alpha_1\beta_2$ interface and reduced proximal strain at the heme.

Traditionally, mechanistic explanations for cooperative binding of ligands to hemoglobin have been based on a ligation-dependent equilibrium between two crystallographically well-defined quaternary structures (*1*). Whereas initially two distinct quaternary structures were identified (R and T), it is becoming increasingly more apparent that there are families of quaternary structures (*2*). In addition, there is evidence of plasticity associated with the tertiary structure in that each of these quaternary structures imposes a boundary for a range of accessible tertiary conformations. The present study explores plasticity within the T quaternary state through measurements that focus on the functional and conformational properties of Fe−Zn hybrid forms of HbA[1] under conditions designed to tune the tertiary structure without inducing a T to R transition.

The Fe−Zn hybrid used in the present study is one of many types of iron−metal hybrids of HbA in which some of the active sites have the heme iron replaced with a metal cation that does not bind specific ligands. Such hybrids have been used to identify α and β chain-specific contributions to spectroscopic and functional properties of the HbA tetramer and to generate half-liganded species useful as models for kinetic intermediates. Furthermore, the choice of metal permits the selection of defined conformations. Metal ions such as Cr(III) (*3*) and Mn(III) (*4*) when incorporated into the heme of HbA mimic the properties of a liganded Fe(II) and thus favor the formation of substantial R state populations of species having ligands only on the Fe-containing subunits. In contrast, when the heme iron is replaced by Zn(II), Mg(II), Ni(II), and Mn(II), the resulting porphyrin more closely resembles the ligand-free ferrous heme and thus favors the formation of half-liganded derivatives having the low-affinity T quaternary state conformation (*4*−*10*). In addition and of specific interest for this study are the Fe−Co hybrids (*11*−*13*). For the unliganded Co porphyrin the metal ion does not lie as far out of the plane of the porphyrin as in deoxyheme or Zn porphyrin, and the Co−proximal histidine bond length is less than that of the Fe(II)−histidine bond (*14*). As a result the heme−F helix separation for subunits with five-coordinate Co-substituted

---

[†] This work was supported through the NIH (PO1GM58890, RO1EB00296, PO1HL71064) and the W. M. Keck Foundation.

[‡] Dedicated to the memory of Eraldo Antonini, eminent biochemist and hemoglobin pioneer, prematurely deceased 20 years ago on March 19, 1983.

* Corresponding author. Tel: (718) 430-3591. Fax: (718) 430-8819. E-mail: jfriedma@aecom.yu.edu.

[§] Albert Einstein College of Medicine.

[||] University of Parma.

[⊥] State University at Buffalo and University at Buffalo VA Medical Center.

[1] Abbreviations: HbA, human adult hemoglobin; Mb, myoglobin; IHP, inositol hexaphosphate; CO, carbon monoxide; GR, geminate recombination; GY, geminate yield; L35, 2-[4-(3,5-dichlorophenylureido)phenoxy]-2-methylpropionic acid; BZF, bezafibrate [2-[4-[2-(4-chlorobenzamido)ethyl]phenoxy]-2-methylpropanoic acid]; ns, nanosecond.

10.1021/bi020648j CCC: $25.00

heme is intermediate between the maximally separated position for five-coordinate Fe(II) or Zn hemes and the minimally separated position for either CO heme, Cr(III) porphyrin or Mn(III) porphyrin. The separation distance between the heme and the F helix appears to correlate with T state stability and reactivity (*14*).

Studies using iron−metal hybrids have raised the issue of conformational and functional plasticity within HbA. In particular, T state forms of HbA having different oxygen binding properties have been identified (*8*). Furthermore, T state ligand binding properties have been shown to be tunable as a function of the specific metal used to generate the hybrid (*14*). The present study seeks to extend such studies to identify the tunable range of both functional and conformational properties.

In this study, we focus on Fe(II)−Zn(II) hybrids of HbA. These hybrids exhibit properties suggesting that functionality within the T state can be tuned, through the addition of allosteric effectors, from the lowest oxygen affinity form of the T state to species exhibiting much higher affinities (*8*). The choice of sample conditions used is designed to trap different functional forms. The crystal studies and the CO combination studies using mixing techniques are used to characterize the extreme low-affinity "end-point" forms. In contrast, the CO recombination studies on sol−gel encapsulated forms of the hybrid that are conformationally trapped (*15*−*20*) as well as on solution phase samples are designed to probe a progression of functionally distinct forms of the intermediate. Measurements of ligand association and recombination (including geminate and solvent phases) as well as oxygen affinity are used to probe functionality. Resonance Raman (visible and UV) spectroscopy is used to explore the conformational properties of these hybrids.

In this study the range of functional and structural properties of the hybrids is tuned using a combination of approaches that includes varying the extent of ligation and the addition of allosteric effectors. Allosteric effectors, such as IHP, BZF, and L35 (abbreviations defined in Materials and Methods), are small non-heme binding molecules that modulate Hb reactivity in part by preferentially binding to the T state and by modifying the functional properties of both the R and T state. Whereas IHP binds in at the DPG binding site ($\beta\beta$ cleft at the terminus of the central cavity) (*21*), both BZF (*22*, *23*) and L35 (*24*) bind in the central cavity (toward the $\alpha\alpha$ end). The overall objective is to determine the extent to which conformation and functionality can be tuned through partial ligation, allosteric effectors, and external constraints that limit ligation or deligation-induced conformational change. The results support a picture in which there is considerable conformational and functional plasticity within the T quaternary structure.

MATERIALS AND METHODS

Materials. Unless otherwise noted, all chemicals and reagents were obtained from commercial suppliers at the highest quality available and were used without further purification. Three different effectors were used in this study: inositol hexaphosphate (IHP), bezafibrate (BZF), and 2-[4-(3,5-dichlorophenylureido)phenoxy]-2-methylpropionic acid (L35), a potent bezafibrate-type effector (*24*), that was obtained as a generous gift from Dr. I. Lalezari.

Preparation of Symmetrical, Fe−*Zn Hybrids of Human HbA. (A) α and β Globins of HbA.* The globin of human HbA was prepared by the acid−acetone precipitation method of Rossi-Fanelli et al. (*25*) as modified and described by Hui et al. (*26*). The precipitated globin was solubilized in 8 M urea and 3 mM DTT in 50 mM phosphate, pH 6.7, buffer and fractionated into its α and β globin components by chromatography in urea buffers on a CM-Sepharose CL-6B column by a modification of the method of Clegg et al. (*27*, *28*) and described by Hui et al. (*26*).

(B) Human Hemoglobin β Chains Containing Zinc Protoporphyrin IX. β[Zn] chains were prepared by reacting β globin with zinc protoporphyrin IX as described by Noble and others (*29*). A buffered solution of β globin in 8 M urea was diluted to 0.3 mg/mL in water, and a 1.2 molar excess of solubilized Zn porphyrin was added. After overnight incubation at 4 °C, the sample was purified by chromatography on a CM-52 column. The yield from this procedure is typically 30%. All preparations and experiments (whenever possible) involving Zn porphyrin were carried out in lights out, semidark conditions.

(C) Human Hemoglobin α Chains Containing Zinc Protoporphyrin IX. α[Zn] chains were prepared by two methods as previously described (*29*). In the first, α globin was reacted with zinc protoporphyrin IX in a procedure similar to that used for the β chains, except purification was by chromatography on a DE-52 column followed by further purification by HPLC using a DEAE Toso Haas column. In the second, α[Zn] chains were prepared by displacing the heme with Zn porphyrin. A solution of α chains was incubated with a 1.5 molar excess of Zn porphyrin at 4 °C overnight, and the free porphyrin was then removed by chromatography on phenyl-Sepharose. Following a total of three such incubations, the replacement of heme by Zn porphyrin was complete.

(D) Preparation of Fe−*Zn Hybrids of Human Hemoglobin.* Symmetrical, Fe−Zn hybrid hemoglobins (either α[Fe]β[Zn] or β[Fe]α[Zn]) were assembled by combining a Zn porphyrin containing chain with a 1.2-fold molar excess of its corresponding heme-containing partner chain, i.e., α[Zn] chains with β[Fe] chains and α[Fe] chains with β[Zn] chains as previously described (*29*). Of critical importance for the validity of this study is the ability to know when and if the probed samples indeed contain tetramer HbA and not dimers which would have different properties. CO recombination kinetics, following photolysis with long pulses of light from photographic strobes (data not shown), clearly show that the propensity for dimer formation of the Fe−Zn hybrids is less than or comparable to that of HbA. On the basis of these findings, the dimer populations were determined to be insignificant under all conditions (including the low concentration conditions used for the combination rate measurements) for which this is true for HbA.

Fe−Zn hybrid samples were stored in the dark at 4 °C. Samples showed no optical or functional indications of degradation subsequent to experiments requiring laser illumination or excitation.

Equilibrium and Kinetic Measurements in Solution. (A) Kinetics of CO Combination with Deoxygenated Hemoglobin by Stopped Flow. Kinetics were measured with an OLIS U.S.A. (On Line Instrument Systems Inc., Bogart, GA) stopped-flow apparatus. The procedures were essentially those of Gibson (*30*) as described by Doyle et al. (*31*). Reactions were carried out at 20 °C in 100 mM HCl/BisTris buffer at pH 7 and were followed at 420 and 435 nm using a 1.7 cm path length cell. Concentrations of CO and hemoglobin (in porphyrin equivalents) were 20 and 2 μM, respectively.

(B) Equilibria of Oxygen Binding to Hemoglobin in Solution. Oxygen-binding curves were measured at 20 °C in 0.1 M HCl/BisTris buffer, pH 7, in the absence and presence of 100 μM IHP by tonometry using the procedure of Allen et al. (*32*), modified by Nagel et al. (*33*), and described by Doyle et al. (*31*). A 500 mL tonometer with an attached 2 mm cuvette was used. The Hb concentration was 160 μM in heme equivalents. To maintain the heme groups in their reduced, ferrous state, the enzyme system of Hayashi et al. (*34*) was utilized.

Equilibrium of Oxygen Binding to Crystals of Deoxygenated Fe−Zn Hybrids of HbA. Crystals of Fe−Zn hybrids of hemoglobin were grown from PEG 8000 M_r solutions at room temperature as previously described (*35*). Once grown, the crystals were washed sequentially with 20% and 36% (w/v) anaerobic PEG 8000 M_r containing 30 mM sodium dithionite and 10 mM potassium phosphate, pH 7.2, and were stored at 20 °C until use (*36*).

Crystals were resuspended one time in a solution containing 34% (w/v) PEG 8000, 10 mM potassium phosphate, 1 mM EDTA, and 30 mM sodium dithionite, pH 7.2, and six times in a dithionite-free deoxygenated solution containing 3000 unit/mL catalase. Crystals were anaerobically loaded in the Dvorak-Stotler flow cell (*37*) that was mounted on the thermostated stage of a Zeiss MPM03 microspectrophotometer (*38*). Crystal orientation and polarized absorption measurements were carried out as previously described (*38*). Due to the light sensitivity of Fe−Zn hybrids, crystals were protected from light and illuminated only with monochromatic light of low intensity.

Polarized absorption spectra were recorded as a function of oxygen pressure. Helium−oxygen mixtures were obtained using an Environics 200 gas mixture generator. Fractional saturation with oxygen and fractional concentration of oxidized hemes were calculated by fitting the observed spectra to the spectra of fully deoxygenated, oxygenated, and oxidized Fe−Zn hybrids (reference spectra) plus a baseline offset (*38*). Reference spectra were obtained by suspending first an Fe−Zn hybrid crystal first in a buffer solution containing dithionite, then in a solution equilibrated with 760 Torr of oxygen at 4.5 °C, and finally in a buffer solution containing 5 mM potassium ferricyanide. Individual crystals were exposed to only one or two oxygen pressures since a fast oxidation was observed. Oxygen binding measurements were carried out at 15 °C, pH 7.2.

Sol−Gel Encapsulation. Both HbA and the hybrids were encapsulated in porous sol−gels using an acid-free variation of the encapsulation protocol of Zink and co-workers (*39*). In this modified protocol, described in detail in earlier work (*19*, *20*), there is no sonication or addition of either acid or alcohol. A key feature of this protocol is the addition of glycerol (25 vol %) to the pH 6.5 buffers used for both gel preparation and gel-sample bathing. This protocol provides a greater degree of conformational "locking" compared with other protocols that have been tried. The diagram below shows two different preparative protocols designed to trap or "lock" different conformations of CO-saturated derivatives of both HbA and the hybrids. The species placed in the brackets are encapsulated prior to aging, whereas those placed outside the brackets are added after gelation and aging. For HbA, protocols 1 and 2 typically yield the R and T state CO derivative of HbA. This basic approach but with different sol−gel recipes has been used by several groups to trap and probe R and T state forms of HbA using oxygen titrations, kinetics, and spectroscopy (*15*−*17*, *19*, *40*, *41*). The gelation protocol used in the present study has also been shown to be successful in limiting CO binding induced tertiary structure changes in myoglobin (Mb) (*20*).

protocol 1: trapping the COHb equilibrium structure

$$\text{COHb} \pm \text{effectors} \xrightarrow{\text{gelation and aging}} [\text{COHb} \pm \text{effectors}]$$

protocol 2: trapping the deoxyHb equilibrium structure

$$\text{deoxyHb} \pm \text{effectors} \xrightarrow{\text{gelation and aging}} [\text{deoxyHb} \pm \text{effectors}] \xrightarrow{\text{CO exposure}} [\text{deoxyHb} \pm \text{effectors}] + \text{CO}$$

In this study sol−gel samples are prepared as a thin layer either on the inner face of a cuvette or on the bottom portion of an NMR tube as previously described (*20*). In all cases the sol−gel sample is bathed in an excess of buffer (50 mM BisTris acetate, pH 6.5, + 25% glycerol). The atmosphere above the buffer is carefully controlled (N_2 or CO). The redox and ligation status of the sol−gel encapsulated samples are monitored using the visible absorption spectrum that is taken before and after either preparative procedures or measurements. The samples are stored at ∼4 °C to minimize relaxation of nonequilibrium populations trapped within the sol−gel (*17*).

Geminate and Solvent Phase Recombination. Geminate and solvent phase recombination after photodissociation by 530 nm Nd:YAG second harmonic 8 ns pulses at 1 Hz was monitored and displayed using a previously described methodology (*20*, *42*). The kinetics, at ∼3 °C, are displayed on a log−log plot of absorbance versus time to better expose the multiple phases that extend over many decades in time. On such a plot an exponential decay appears as a horizontal line that abruptly changes to a near vertical line that intercepts the time axis at a point that is approximately the reciprocal of the exponential time constant. Kinetics derived from a large continuous distribution of exponentials (distributed kinetics) appear as a sloping straight line. Such behavior is observed for ligand rebinding at cryogenic temperatures or highly viscous solutions (*43*, *44*).

Visible Resonance Raman. Soret- enhanced resonance Raman spectra were generated from the deoxy and half-liganded iron metal hybrids using 436 nm 8 ns pulses at 20 Hz. For the half-liganded derivatives, these pulses both photodissociated the CO and generated the spectrum of the 8 ns photoproduct. The apparatus used for generating these spectra is described in detail in earlier publications (*45*). In all cases the spectra are generated from scattering off a thin layer of sample contained in a spinning NMR tube maintained at ∼4 °C.

UV Resonance Raman. The 229 nm excited resonance Raman spectra of Fe−Zn hybrid hemoglobins were generated

Table 1: Averages of Kinetic Data for the Reactions of the Fe−Zn Hybrid with CO

	l'_1 (μM^{-1} s^{-1})	l'_2 (μM^{-1} s^{-1})
α(Fe)β(Zn)		
−IHP	0.13	0.10
+IHP	0.10	0.10
α(Zn)β(Fe)		
−IHP	0.11	0.09
+IHP	0.046	0.036

at ~4 °C using previously described instrumentation and protocols (*18*, *45*).

Variance in Experimental Conditions. Care was taken to ensure consistent experimental conditions among the different experimental protocols; however, some variance, most notably in the temperature and in some cases pH as well as buffer, was unavoidable due both to the required conditions of the individual techniques and of experimental setups and to the need to compare certain results to earlier measurements using established protocols.

RESULTS

CO Combination Kinetics. The kinetics of CO combination with the deoxygenated derivatives of the α[Zn]β[Fe] and α[Fe]β[Zn] hybrids have been examined at pH 7 in the presence and absence of 100 μM IHP. Unlike the reaction of CO with deoxygenated HbA, which is accelerating or autocatalytic, CO binding to the Fe−Zn hybrids exhibits apparent second-order rate constants which decrease to variable extents as the reactions proceed. Since the heme moieties in a symmetrical hybrid are expected to be identical prior to the attachment of the first ligand molecule, these kinetics were fitted to a sequential reaction mechanism as shown in eq 1. The results are reported in Table 1. In the

$$\mathrm{HbZn_2Fe_2} + 2\mathrm{CO} \xrightarrow{2l'_1} \mathrm{HbZn_2FeFeCO} + \mathrm{CO} \xrightarrow{l'_2} \mathrm{HbZn_2(FeCO)_2} \quad (1)$$

absence of IHP the two hybrid molecules bind CO with very similar kinetics. In both cases the kinetic scheme of eq 1 gave a good fit to the data. The results suggest that the binding of CO at one of the hemes reduces the rate of CO binding to the second, equivalent heme by about 25%. The effects of IHP addition are significantly different for the two hybrids. For the α[Fe]β[Zn] hybrid IHP has no effect on l'_2 but reduces l'_1 to the value of l'_2, resulting in a kinetically homogeneous reaction. In contrast, IHP reduces both l'_1 and l'_2 of the α[Zn]β[Fe] hybrid. The effect on l'_1 is greater than seen with the α[Fe]β[Zn] hybrid, and the fractional reduction in l'_2 is even greater.

Equilibrium of Oxygen Binding FeZn Hybrids in Solution. Binding equilibria for the reactions of oxygen with α[Zn]β[Fe] and α[Fe]β[Zn] hemoglobins were determined at 20 °C and pH 7 in the presence and absence of IHP as described in Materials and Methods. Because of the relatively low oxygen affinities and low cooperativity of these hemoglobins, they are not saturated at 1 atm of pure oxygen, with the result that the spectrum of the oxygen-saturated protein was not available. Although this would present a serious problem in the analysis of the binding of oxygen to the four hemes of HbA, the two-step Adair equation for the equilibrium of ligand binding to two initially identical sites can be easily solved without this information. Using the Levenberg−Marquart fitting procedures found in Sigma Plot (SPSS), the dissociation constants for the two binding steps, K_1 and K_2, are obtained. The p_{50} is then calculated as the square root of the product of the two dissociation constants. The p_{50} is the relevant parameter for comparison with the p_{50} of the hybrids in T state crystals. The results of these calculations are presented in Table 2. A reasonable standard error for the p_{50} in Table 2 is 10%. Therefore, in the absence of IHP the oxygen affinities of the two hybrids are not significantly different, but the oxygen affinity of α[Zn]β[Fe] appears to be reduced more by the addition of IHP than is that of α[Fe]β[Zn]. No significant cooperativity is observed in the binding of oxygen to these hybrids. The slightly negative cooperativity found for the α[Zn]β[Fe] hybrid in the presence of IHP is at the boundaries of significance.

Table 2: Oxygen Affinities of FeZn Hybrids of HbA

sample	IHP	K_1	p_{50}	n
α[Fe]β[Zn]	−	75	67	1.04
α[Zn]β[Fe]	−	70	67	1.02
α[Fe]β[Zn]	+	138	131	1.02
α[Zn]β[Fe]	+	156	182	0.93

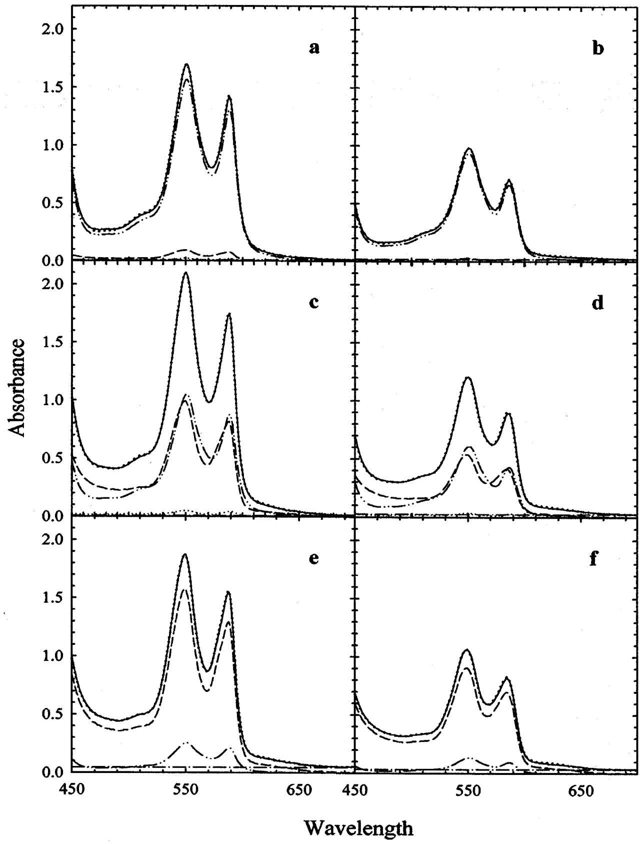

FIGURE 1: Polarized absorption spectra of α[Fe]β[Zn]. Polarized absorption spectra (large dotted line) were recorded on different crystals at 7 (a, b), 75 (c, d), and 760 Torr (e, f) along the *a* (a, c, e) and *c* (b, d, f) directions. The calculated spectra (solid line) and the deoxygenated (dashed−dotted−dotted−dashed line), oxygenated (dashed line), and oxidized (dotted line) hybrid spectra are shown plus the baseline (dashed−dotted−dashed line). The fractional saturations with oxygen are 0.06 (a), 0.04 (b), 0.51 (c), 0.48 (d), 0.87 (e), and 0.88 (f).

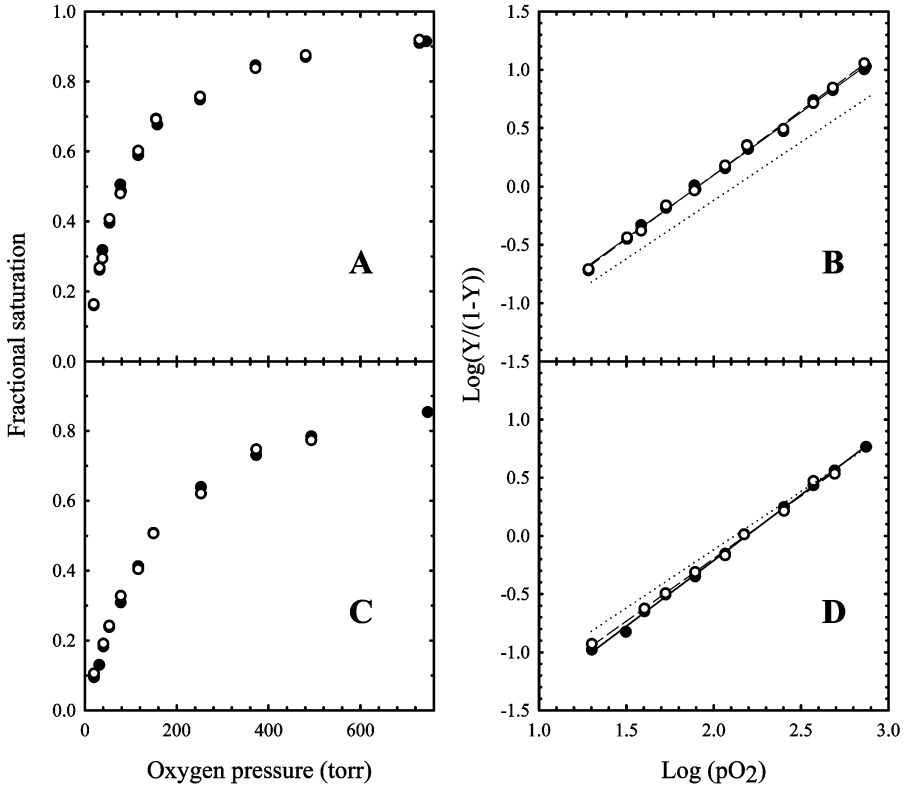

FIGURE 2: Oxygen binding curve and Hill plot of α[Fe]β[Zn] (A, B) and α[Zn]β[Fe] (C, D) crystals. (A) Fractional saturation with oxygen along the *a* (closed circle) and *c* (open circle) directions. (B) Hill plot of data shown in panel A. The straight lines are the fittings through points collected along the *a* (solid line) and c (dash line) directions. The p_{50} values are 81.4 ± 1.5 and 81.3 ± 1.5, respectively, and the Hill coefficients are 1.08 ± 0.02 and 1.10 ± 0.02, respectively. (C) Fractional saturation with oxygen along the *a* (closed circle) and *c* (open circle) directions as a function of oxygen pressure. (D) Hill plot of data shown in panel C. The straight lines are the fittings through points collected along the *a* (solid line) and *c* (dashed line) directions. The p_{50} values are 154.6 ± 2.2 and 152.2 ± 3.3, respectively, and the Hill coefficients are 1.13 ± 0.01 and 1.08 ± 0.02, respectively. In panels B and D, the dotted line is the Hill plot of HbA crystals (*81*).

Equilibrium Measurements of Oxygen Binding to Crystalline Hemoglobin. A representative set of polarized absorption spectra recorded at different oxygen pressures, the corresponding calculated spectra, and the component reference spectra for Fe–Zn hybrids of HbA are shown in Figure 1. The quality of the fitting is so good that observed and calculated spectra are indistinguishable. The oxygenation curves in Figure 2 indicate that α[Fe]β[Zn] hybrid crystals (panels A and B) exhibit a p_{50} of 81.4 and 81.3 Torr along the *a* and *c* crystal axes, and the α[Zn]β[Fe] hybrid crystals (panels C and D) exhibit a p_{50} of 154.6 and 152.2 Torr along the *a* and *c* crystal axes. The corresponding Hill coefficients for α[Fe]β[Zn] hybrid crystals are 1.08 and 1.10 and for α-[Zn]β[Fe] hybrid crystals are 1.13 and 1.08.

Geminate and Bimolecular Recombination. Figure 3 shows the rebinding of CO to the α[Zn]β[FeCO] hybrid in solution after photodissociation using an 8 ns photolysis pulse. The rebinding trace for photodissociated COHbA is included as reference to indicate anticipated behavior for different rebinding phases. The initial rebinding occurring throughout the nanosecond time regime has been identified as geminate recombination (*46*–*48*). The two recombination phases observed for COHbA occurring between 100 μs and 1 s correspond to the bimolecular rebinding of CO molecules from the solvent (*49*). The fast and slow bimolecular phases correspond to R and T state combination rates, respectively.

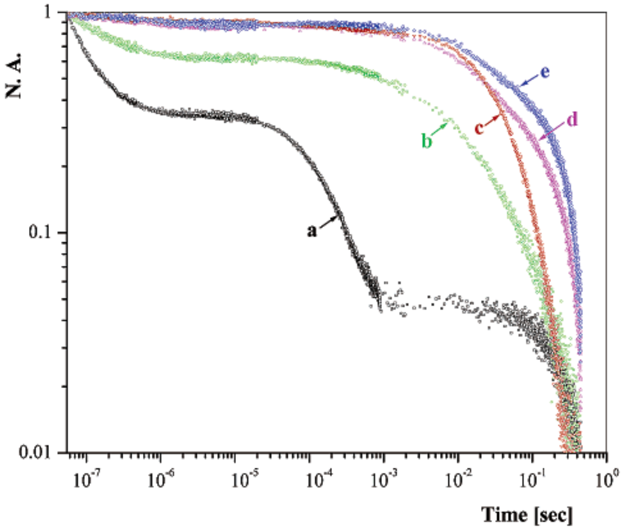

FIGURE 3: Geminate and bimolecular rebinding displayed on a log–log plot of normalized absorbance versus time for COHbA and α[Zn]β[FeCO] in pH 6.5 (50 mM BisTris acetate) solution at 3.5 °C. Plots: (a) COHbA; (b) α[Zn]β[FeCO]; (c) α[Zn]β[FeCO] + IHP (8× excess over tetramer); (d) α[Zn]β[FeCO] + L35; (e) α-[Zn]β[FeCO] + IHP + L35.

It can be seen that even in the absence of IHP and/or L35, the geminate recombination for the hybrid is substantially less than for HbA. The geminate yield (GY) drops from ∼65% to 35%. The addition of IHP and/or L35 further reduces the geminate yield. The most rapid second-order process in hemoglobin is the recombination within the R conformational state as seen for HbA. This R state rebinding does not begin until well after 10 μs following photolysis.

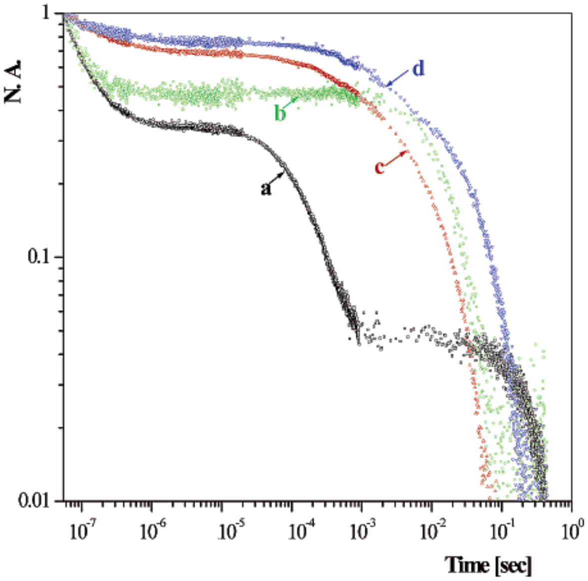

FIGURE 4: Geminate and bimolecular rebinding displayed on a log−log plot of normalized absorbance versus time for COHbA and α[FeCO]β[Zn] in pH 6.5 (50 mM BisTris acetate) solution at 3.5 °C. Plots: (a) COHbA; (b) α[FeCO]β[Zn]; (c) α[FeCO]β[Zn] + IHP(8× excess over tetramer); (d) α[FeCO]β[Zn] + IHP + L35.

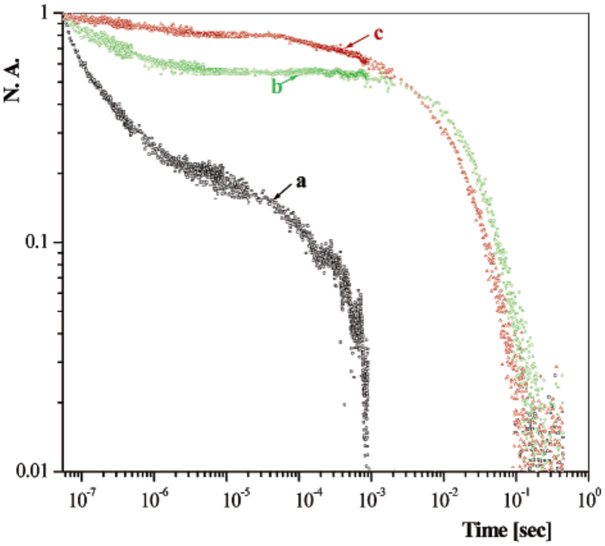

FIGURE 5: Geminate and bimolecular rebinding displayed on a log−log plot of normalized absorbance versus time for sol−gel encapsulated COHbA and α[Zn]β[FeCO] bathed in pH 6.5 (50 mM BisTris acetate) buffer + 25% glycerol at 3.5 °C. Plots: (a) encapsulated COHbA; (b) encapsulated α[Zn]β[FeCO]; (c) encapsulated α[Zn]β[FeCO] + IHP (8× excess over tetramer).

If we accept that all processes occurring before 10 μs are geminate, then in the presence of IHP and/or L35 the geminate yield for the α[Zn]β[FeCO] hybrid varies from 10% to 15%. Unlike COHbA, where two bimolecular phases are clearly discernible, for the α[Zn]β[FeCO] hybrid, only a single phase is evident. However, the single phase is nonexponential. On a log−log plot, a homogeneous exponential reaction takes place over approximately 2 decades on the log time axis. The second-order process in curve b occupies some 3.5 decades. Although the kinetics eventually slows to that of the T state, a significant proportion of the reaction takes place in the time regime normally assigned to the R state, between 10^{-5} and 10^{-3} s. Addition of IHP and/or L35 reduces the amount of reaction occurring in this time window but does not eliminate it. Half-liganded iron−cobalt hybrids behave differently. In contrast to the altered rebinding behavior observed for the effector-free α[Zn]β[FeCO] hybrid, the geminate yield and the bimolecular kinetics (trace not shown) for the effector-free α[Co]β[FeCO] hybrid are very similar to those shown for COHbA.

Figure 4 shows the geminate and bimolecular recombination of CO to the α[FeCO]β[Zn] hybrid, and as in Figure 3, the kinetic trace for COHbA is again included for comparison. The kinetic patterns are similar to those seen for the α[Zn]β[FeCO] hybrid but with some differences. In the absence of IHP and/or L35, the geminate yield is greater for this hybrid (∼52% versus 35%) but still less than for HbA. Furthermore, although the addition of IHP and/or L35 reduces the geminate yield as seen for the α[Zn]β[FeCO] hybrid, in this case the combined presence of IHP and L35 is required to achieve the maximum reduction in geminate yield. Unlike the α[Zn]β[FeCO] hybrid where the GY drops to roughly 10%, for this mutant there is still an observable GY of 20−30% under similar conditions. As with the α[Zn]β[FeCO] hybrid, only a single phase is observed for the bimolecular recombination either with or without IHP and/or L35, and the single phase ends with a T state recombination rate. Although in the absence of IHP the second-order process appears to be quite homogeneous, in the presence of IHP or IHP + L35 the reaction becomes heterogeneous. Not shown are the recombination kinetics from an effector-free sample of α[FeCO]β[Co]. The kinetic trace is very similar (partially reduced GY and the absence of a distinct R state bimolecular combination phase) to that of the corresponding α[FeCO]β[Zn] sample.

Figure 5 shows the kinetic traces for the recombination of CO after the photodissociation of samples of the α[Zn]β[FeCO] hybrid that are encapsulated in a porous sol−gel matrix. The corresponding trace for sol−gel encapsulated COHbA is also shown. As previously reported (*19*), the recombination for sol−gel encapsulated COHbA consists of an enhanced geminate phase (increased geminate yield compared to a comparable solution phase samples) and a single fast solvent phase that corresponds to the R state bimolecular rebinding. The enhanced geminate yield is not seen for COHbA encapsulated using other gelation protocols that do not have the added glycerol (*19*, *40*). This enhancement is likely the result of a higher internal viscosity within the glycerol containing sol−gel (*20*, *50*). A comparison with Figure 3 reveals that the kinetic pattern observed in solution is similar to that seen for the encapsulated α[Zn]β[FeCO] hybrid. The geminate yield, in both the presence and absence of IHP, is somewhat larger in the sol−gel, but the geminate traces are similar in form. However, in the absence of IHP the encapsulated α[Zn]β[FeCO] exhibits little or no reaction in the 10^{-5}−10^{-3} s time window and is quite homogeneous. This is in contrast to recombination in solution in the absence of IHP (Figure 3) where heterogeneity is observed. The α[Zn]β[FeCO] hybrid encapsulated in the presence of IHP exhibits a significant recombination reaction in the same time interval, just as is observed for the hybrid in solution in the presence of IHP. The kinetic trace (not shown) for a sample that was initially encapsulated as the fully deoxygenated derivative of the α[Zn]β[Fe] hybrid and converted to the CO derivative after a period of aging is virtually identical

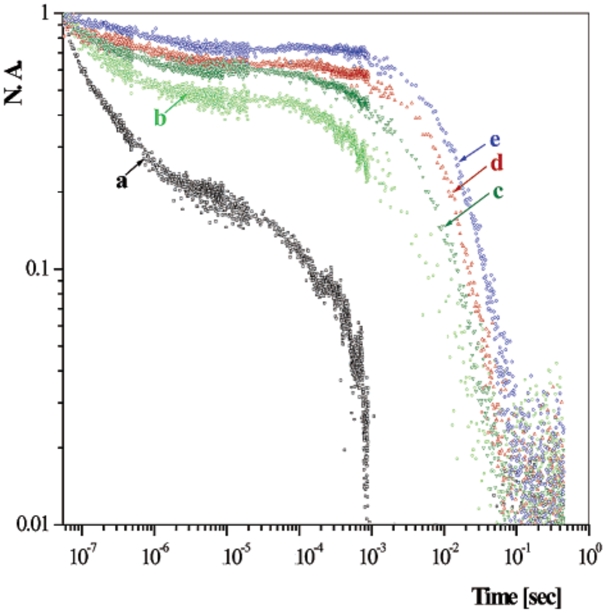

FIGURE 6: Geminate and bimolecular rebinding displayed on a log−log plot of normalized absorbance versus time for sol−gel encapsulated COHbA and α[FeCO]β[Zn] bathed in pH 6.5 (50 mM BisTris acetate) buffer + 25% glycerol at 3.5 °C. Plots: (a) encapsulated COHbA; (b) encapsulated α[FeCO]β[Zn]; (c) encapsulated deoxy α[Fe]β[Zn] to which CO is added after aging; (d) encapsulated α[FeCO]β[Zn] + IHP + L35; (e) encapsulated deoxy α[Fe]β[Zn] + IHP + L35 to which CO is added after aging.

to that shown in Figure 5 for the sample of α[Zn]β[FeCO] encapsulated in the presence of IHP.

Figure 6 shows the kinetic traces for the recombination of CO in samples of the encapsulated α[FeCO]β[Zn] hybrid. The traces from the encapsulated samples mirror those obtained from the corresponding solution phase samples. However, there is also a slight difference. In solution, in the absence of IHP and/or L35, no recombination reaction is observed in the time window of the typical second-order recombination with the R state between 10^{-5} and 10^{-3} s. In the gel in the absence of IHP significant reaction occurs in this time interval, whether the sample is encapsulated as the deoxygenated (d) or the CO (b) derivative. In the latter case 70% of the total recombination is complete by 10^{-3} s, but still the total process ends with the T state rate of recombination, and no clear transition between R state and T state processes, as seen with CO HbA in solution, is observed. Encapsulation in the presence of IHP or L35, whether as the deoxygenated or CO derivative, reduces both geminate rebinding and the amount of reaction occurring in the 10^{-5}−10^{-3} s window.

Visible Resonance Raman (VRR) Spectra: Fe−Proximal Histidine Stretching Frequency. The stretching frequency of the iron−proximal histidine stretching mode, ν(Fe−His), observed in the Soret Band enhanced resonance Raman spectra of equilibrium and nonequilibrium forms of five-coordinate ferrous derivatives of hemoglobins is highly responsive to tertiary structure (*11*, *51*−*59*). For HbA, the frequency of ν(Fe−His) increases in the following sequence: deoxy T state (214 cm^{-1}), photoproduct T (220−225 cm^{-1}) ≈ deoxy R, photoproduct R (230 cm^{-1}). The frequency is in effect a strain gauge reflecting proximal strain or proximal enhancement at the heme (*58*). Proximal strain refers to the additional energy cost of moving the iron into the heme plane upon ligand binding due to the coupling of the globin to the iron coordinate. Proximal enhancement refers to a globin-mediated reduction in the energy cost of moving the iron in plane (*57*, *60*). Proximal strain is associated with a reduced frequency ($<$220 cm^{-1}), whereas enhanced frequencies ($>$220 cm^{-1}) reflect proximal enhancement. In general, increases in this frequency correlate with increases in the geminate yield (*54*, *57*, *59*−*61*).

Table 3: Visible Resonance Raman Data: ν(Fe−His) Band Peak Position (cm^{-1})

solution	deoxy	deoxy IHP	deoxy IHP + L35	CO 8 ns photoproduct	CO 8 ns photoproduct IHP	CO 8 ns photoproduct IHP + L35
HbA	214			230	225	
α[Zn]β[Fe]	220.5	220.2	220.2	230	223.9	223.3
α[Fe]β[Zn]	204[a]			228.6	226	221.5
α[Co]β[Fe]				230		
α[Fe]β[Co]				224.5		

gels	encapsulated deoxy[b]	encapsulated deoxy[b] IHP[d]	encapsulated deoxy[b] IHP + L35[d]	encapsulated deoxy turned CO[c]	encapsulated deoxy turned CO[c] IHP[d]	encapsulated deoxy turned CO[c] IHP + L35[d]
HbA	214	214	215	218.6−226.4	219−223.9	219−222
α[Zn]β[Fe]		220.5				
α[Fe]β[Zn]		205			212.3[a]	

[a] Broad band. [b] Samples of deoxyHbA with and without effectors encapsulated in a sol−gel. [c] Samples where deoxy-liganded HbA with and without effectors are encapsulated in a sol−gel and kept deoxy during gelation and aging of the gel, thereby trapping the deoxy conformation. Only after aging were the gels exposed to CO. The measurements are of the 8 ns photoproduct. [d] Effectors present before and during gelation and while aging the sol−gel sample, as well as in the bathing buffer.

Table 3 contains the peak frequencies of ν(Fe−His) for samples of the [Fe][Zn] hybrid hemoglobins in both solution and sol−gel matrices. The frequencies given are from both the equilibrium deoxy derivatives and the 8 ns photoproduct (derived from CO-saturated derivatives). Also included for comparison are the frequencies obtained from several HbA samples under similar conditions and from the photoproduct of half-liganded iron−cobalt Hb hybrids. Representative series of a low-frequency segment of the full VRR spectra are shown in Figures 7−9. This segment includes ν(Fe−His) as well as several bands sensitive to the inner core of the porphyrin and the heme propionates.

The frequencies of ν(Fe−His) for the deoxy derivatives are very similar to those reported earlier for the corresponding deoxy [Fe][Co] hybrid forms of HbA with the frequency of ν(Fe−His) being higher by approximately 15 cm^{-1} for the β(Fe) subunits relative to the α(Fe) subunits (*13*). It is noteworthy that, for the fully deoxy derivatives of Fe−Zn hybrids, the frequency of ν(Fe−His) for the β heme is seemingly insensitive to the addition of IHP and/or L35 and thus remains substantially higher in frequency than ν(Fe−His) for the α heme under all conditions. In the present study, the low intensity and broad line shape makes a precise determination of the peak frequency of ν(Fe−His) for the α heme difficult (∼205 cm^{-1}); nevertheless, it is substantially lower than that of the β heme (220 cm^{-1}) and similar to the α heme result seen for the [Fe][Co] hybrids (*13*).

Unlike the deoxy derivatives, the symmetric half-liganded CO derivatives of the [Fe][Zn] hybrids exhibit a marked

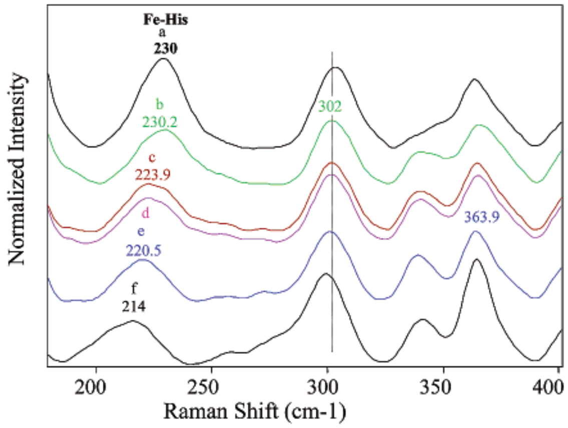

FIGURE 7: Visible resonance Raman spectra of deoxy and photoproduct derivatives of α[Zn]β[Fe] and HbA in solution (BisTris acetate, pH 6.5, at approximately 4 °C): (a) 8 ns photoproduct of COHbA; (b) 8 ns photoproduct of α[Zn]β[FeCO]; (c) α[Zn]β[FeCO] + IHP (8× excess over tetramer); (d) 8 ns photoproduct of α[Zn]β[FeCO] + IHP + L35; (e) deoxy derivative of α[Zn]β[Fe]; (f) deoxyHbA. The intensities of the spectra are normalized to the ν_7 band (~762 cm^{-1}).

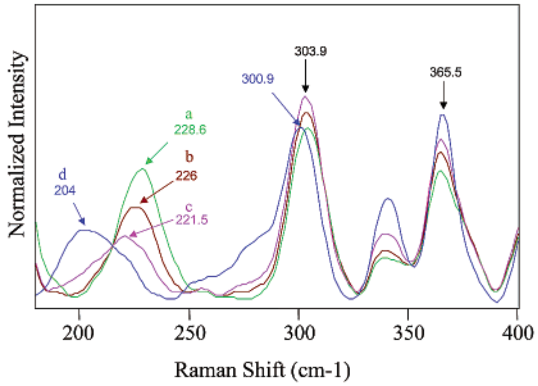

FIGURE 8: Visible resonance Raman spectra of deoxy and photoproduct derivatives of α[Fe]β[Zn] hybrid HbA in solution (BisTris acetate, pH 6.5, at approximately 4 °C): (a) 8 ns photoproduct of α[FeCO]β[Zn]; (b) 8 ns photoproduct of α[FeCO]β[Zn] + IHP (8× excess over tetramer); (c) 8 ns photoproduct of α[FeCO]β[Zn] + IHP + L35; (d) deoxy derivative of α[Feβ[Zn] + IHP. The intensities of the spectra are normalized to the ν_7 band.

response to the addition of IHP and/or L35 as reflected in the frequency of ν(Fe−His) for the 8 ns photoproduct. It can be seen in Figures 7 and 8 that both photoproducts exhibit a ν(Fe−His) that is close in frequency to the 230 cm^{-1} that is observed for the photoproduct of COHbA (*11*, *52*, *54*, *55*, *59*, *62*). The photoproduct of the α[Zn]β[FeCO] hybrid yields a frequency that is very nearly the same as for COHbA; however, for the hybrid, the relative intensity with respect to other Raman bands is lower, and the line shape is skewed toward lower frequencies. The photoproduct of α-[FeCO]β[Zn] yields a slightly lower frequency for ν(Fe−His), 228 cm^{-1} vis à vis 230 cm^{-1}. These high frequencies are typically associated with the photoproduct of the liganded R state of HbA; however, as will be discussed below, the kinetics and UV resonance Raman results suggest that, in the case of the hybrids, the high frequency is associated with a T state population having a highly perturbed tertiary structure relative to that of deoxyHbA.

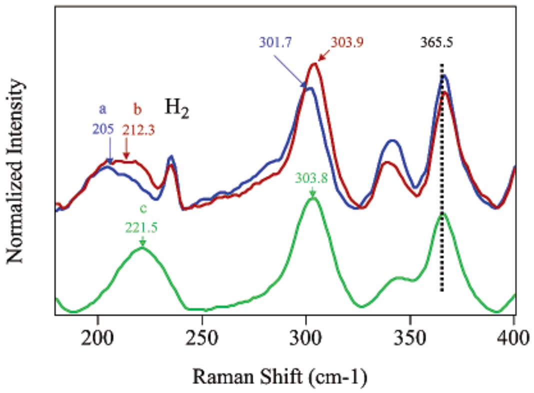

FIGURE 9: Visible resonance Raman spectra of deoxy derivatives of α[Fe]β[Zn] and HbA encapsulated in a sol−gel matrix: (a) deoxy derivative of α[Fe]β[Zn] encapsulated in the presence of IHP; (b) 8 ns photoproduct spectrum of a sample of α[Fe]β[Zn] initially encapsulated as the deoxy derivative in a sol−gel matrix in the presence of IHP to which CO is added after the sample had aged for several days; (c) 8 ns photoproduct spectrum of a sample of HbA initially encapsulated as the deoxy derivative in a sol−gel matrix in the presence of IHP to which CO is added after the sample had aged for a several day period. The intensities of the spectra are normalized to the ν_7 band.

The addition of IHP lowers the frequency of ν(Fe−His) for both photoproducts but with more impact on the α[Zn]β-[FeCO] hybrid. The peak frequencies do not fully convey the effect since the quality of the spectra makes it difficult to accurately evaluate peak positions. A direct superposition of spectra reveals line shape patterns that allow for a clearer assessment of peak shifts. The combined effect of IHP and L35 lowers both frequencies still further to an end-point value of ~222 cm^{-1} for both hybrids. It can be seen that, in the presence of both IHP and L35, the ν(Fe−His) frequency for the α[Zn]β[FeCO] hybrid is nearly the same for the deoxy derivative and for the photoproduct. In contrast, the frequency difference between the deoxy derivative and photoproduct of the α[FeCO]β[Zn] hybrid remains substantial under all conditions even though the difference does decrease from ~23 to ~15 cm^{-1} with the addition of IHP and L35. A pattern of decreasing photoproduct frequency for ν(Fe−His) with addition of IHP and/or L35 is also observed for COHbA but with a reduced response as noted in Table 3. A detailed treatment of the response of COHbA to the addition of allosteric effectors will be the subject of a future publication. It can also be seen that the frequency for the photoproducts of the α[FeCO]β[Co] and the α[Co]β[FeCO] hybrids corresponds respectively to the lowest and highest values observed for the FeZn hybrids.

The VRR spectra of sol−gel encapsulated derivatives of the α[Fe]β[Zn] hybrid are shown in Figure 9. On the basis of earlier studies (*15*−*17*, *19*, *20*, *41*, *60*, *63*) it is anticipated that the encapsulated deoxy derivatives will retain their initial quaternary state after the samples are exposed to CO. It can be seen that the spectrum of the encapsulated deoxy derivative is very similar to that of the corresponding solution phase deoxy sample. The spectrum of the encapsulated deoxy sample + IHP turned CO after aging (protocol 2) yields a ν(Fe−His) band that is broad with a frequency distribution that spans the values of the equilibrium deoxy derivative through those of the photoproduct plus effectors seen in solution. For comparison, the figure also displays the photoproduct spectrum of [deoxyHbA] + CO (protocol 2). It can be seen that the frequency of ν(Fe−His) is at ~220 cm^{-1} as previously reported (*20*). Similar frequencies are observed (not shown) for samples of [deoxyHbA + IHP ± L35] + CO but with the IHP + L35 containing sample having a slightly higher frequency (222 cm^{-1}). In contrast, the corresponding frequency from the photoproduct of [COHbA] (protocol 1) is the same as in solution at 230 cm^{-1}.

Visible Resonance Raman (VRR) Spectra: γ_7. The VRR spectra show that the Raman band at ~300 cm^{-1}, which arises from the heme γ_7 mode, exhibits subunit-specific behavior with respect to CO binding induced changes. This mode is associated with an out of plane motion of the heme methine carbons, and its Raman frequency decreases with increasing strain in the heme (*64*). The frequency of this Raman band is observed to increase by ~3 cm^{-1} in going from the equilibrium deoxy T form of HbA to the photoproduct of COHbA. The spectra presented above show that this shift is due almost exclusively to changes in the α subunit. The presented results also show that this shift occurs when CO binds to the α heme for both R and T state structures. Earlier analysis of the subunit-specific behavior of this mode in deoxyHbA (*64*), in conjunction with the present findings, indicates that when the deoxy α heme undergoes ligation even within the T state, there occurs a protein conformational change that reduces heme-associated strain.

UV Resonance Raman (UVRR) Spectra. (A) UVRR Spectra: Overview. All but one of the figures in this section show only the high-frequency region (1500−1660 cm^{-1}) of the full UVRR spectrum (800−1680 cm^{-1}). This high-frequency region contains bands that have been well characterized with respect to conformational degrees of freedom. The weak band at 1512 cm^{-1} has recently been reassigned as the 2xW18 overtone mode (*65*). This band shows a decrease in intensity when HbA switches from the T state to the R state (*66*, *67*, *74*). This intensity change is likely related to Trp β37 in the switch region of the $\alpha_1\beta_2$ interface on the basis of its behavior in the HbAβ37Trp → Glu mutant (*45*). The W3 band at ~1558 cm^{-1} has two contributions (*58*, *66*−*68*). The central feature that peaks at ~1558 cm^{-1} is derived from the two A helix tryptophans (α14 and β15) whereas the R−T sensitive shoulder at ~1550 cm^{-1} originates from Trp β37. The intensity of this shoulder is reflective of the R−T sensitive hinge region of the $\alpha_1\beta_2$ interface. The tyrosine-derived Y8a band at ~1616 cm^{-1} shows an ~2 cm^{-1} shift to higher frequency when liganded R state HbA is converted to the deoxy T state (*66*, *67*). This frequency shift originates primarily from Tyr α42 (*58*, *69*−*71*) in the switch region of the $\alpha_1\beta_2$ interface.

(B) UVRR Spectra of the Deoxy Derivatives of the [Fe]-[Zn] Hybrids. The Raman bands in the 229 nm excited UVRR spectra of the deoxy derivatives of both Fe−Zn hybrids (not shown) were essentially identical in frequency and intensity to the corresponding bands in the spectrum of deoxyHbA under the same solution and concentration conditions. In the subsequent figures, the UVRR spectrum of deoxyHbA is used as the deoxy T state reference spectrum.

(C) UVRR Spectra of the CO-Saturated Derivatives of the α[Zn]β[Fe] Hybrid. Figure 10 shows both the UVRR spectra of deoxyHbA and the CO-saturated derivative of the α[Zn]β-[FeCO] hybrid + IHP (both normalized to the selenate Raman band at approximately 850 cm^{-1}) and the difference spectrum obtained by subtracting the later from the former. Also included is the deoxy minus CO difference spectrum for HbA that serves as the reference for the difference spectrum between the deoxy T and liganded R conformations as accessed for HbA. It can be seen from the difference spectra that whereas there are clear-cut frequency shifts associated with the HbA spectra (e.g., Y8a), there are no major frequency shifts for the hybrid. The difference spectrum involving the hybrid reveals that several bands have lower intensity relative to the deoxyHbA spectrum. Overall, the spectrum of α[Zn]β[FeCO] + IHP resembles that of deoxyHbA but with reduced intensity in most bands. The general reduction in the intensity of the spectrum derived from the CO-saturated hybrids relative to the spectrum of deoxyHbA is also apparent for most of the other hybrid samples; however, several of the samples do show additional spectral changes that are typically associated with elements of the R state $\alpha_1\beta_2$ interface. The following three figures are designed to feature these sample-dependent differences in the UVRR spectra.

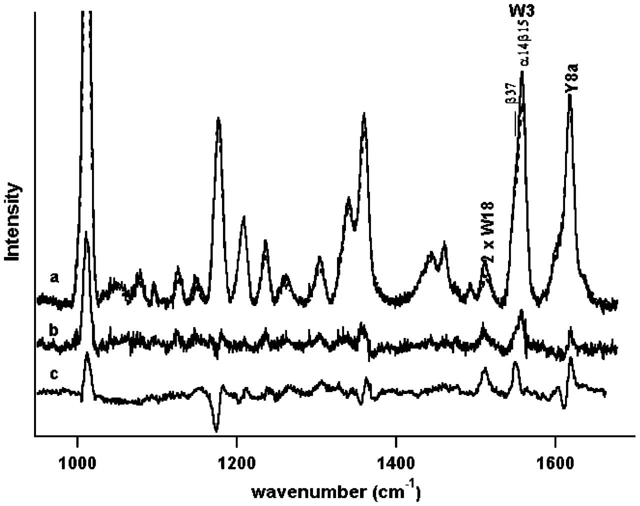

FIGURE 10: 229 nm excited UV resonance Raman (UVRR) spectra of the deoxy and CO derivatives of HbA and α[Zn]β[Fe] in solution at pH 6.5 (50 mM BisTris acetate): (a) deoxyHbA (solid line) and α[Zn]β[FeCO] + 8× excess IHP over tetramer; (b) UVRR difference spectrum for deoxyHbA − α[Zn]β[FeCO] + IHP; (c) UVRR difference spectrum for deoxyHbA − COHbA.

Figure 11 shows, as a function of added allosteric effector, a comparison of the high-frequency segment (1500−1650 cm^{-1}) of the UVRR spectrum for α[Zn]β[FeCO] with the corresponding spectrum segment from deoxyHbA. Included is the difference spectrum generated by subtracting the hybrid spectrum from the deoxyHbA spectrum. The spectra in panels a−c are normalized with respect to the selenate internal standard. The figure shows the progression in going from effector-free (a) to added IHP (b) to added IHP + L35 (c). Panel d shows the corresponding comparison between deoxyHbA and COHbA.

Panel c shows that the intensity of the 2xW18 band at ~1510 cm^{-1} and the Y8a band for the α[Zn]β[FeCO] in the presence of IHP and L35 is very similar to that of the corresponding bands of the deoxyHbA sample. The similar intensity of the 2xW3 bands and the absence of a shift in the Y8a band (the broad contribution between 1590 and 1610 cm^{-1} is due to the Raman from the added L35) are consistent with a T state conformation for the hybrid under these conditions. The enhanced intensity for the β37 shoulder of the W3 band is beyond the intensity enhancement expected

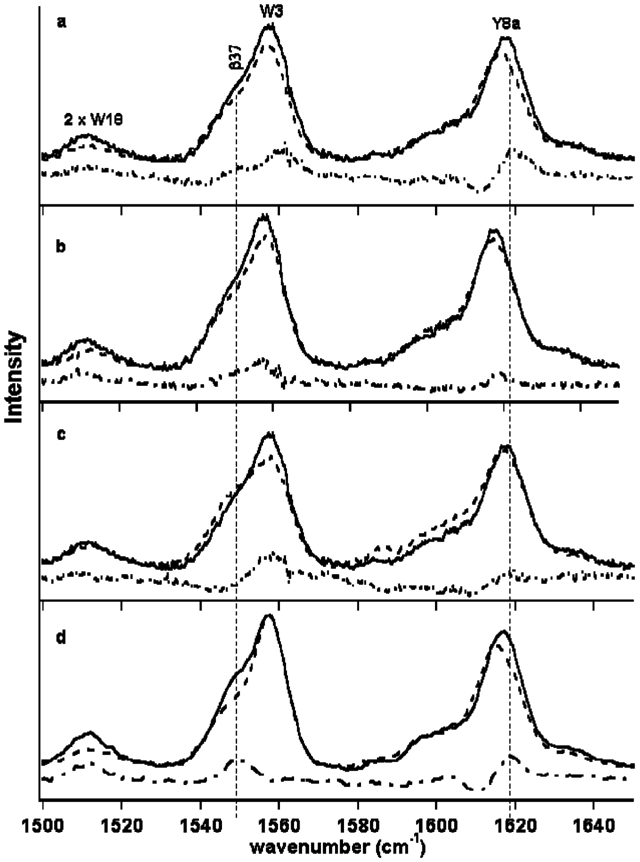

FIGURE 11: High-frequency segment of the UVRR spectrum and the corresponding difference spectrum for solutions (as in Figure 10) of HbA and α[Zn]β[FeCO]. In all of the panels the solid line is the result for deoxyHbA. In panels a−c, the dashed line represents α[Zn]β[FeCO] with (a) no effectors, (b) 8-fold excess of IHP, and (c) excess IHP and L35. In panel d, the dashed line is the result for COHbA. In all panels the difference spectrum is the result of subtracting the CO-liganded spectrum from the deoxyHbA spectrum.

for a T species based on deoxyHbA (without L35). Preliminary results (Juszczak and Friedman, unpublished results) from other Hb derivatives indicate that this further intensity increase is due to a direct effect of L35 on Trp β37 occurring through the interaction of L35 with central cavity residues, which are likely to include Asp α94, Trp β37, and nearby waters. The indole ring of Trp β37 is hydrogen bonded to Asp α94. It is the variation in that interaction that is responsible for the conformation dependence of the 1550 cm^{-1} shoulder of W3.

The reduced relative intensity of the central peak of the W3 band at 1558 cm^{-1} reflects a weakened hydrogen bond between one or both of the A helix tryptophans (α14, β15) and their hydrogen-bonding partner on the E helix. On the basis of the analysis of other Hb samples showing similar behavior (*72*−*76*), it is likely that the change is due to the combined effect of partial ligation and the addition of IHP, and L35 is causing a collapse of at least one of the E helices away from the A helix. A reduction in the intensity of the central peak of the W3 band without noticeable alteration of the T state signatures (Y8a and the β37 shoulder of W3) was also observed to be the first UVRR change occurring upon addition of CO to a cooled sol−gel encapsulated sample of deoxyHbA. This similarity suggests that α[Zn]β[FeCO] in the presence of IHP and L35 resembles the very first intermediate in the ligation-induced transition from deoxy T to liganded R HbA.

In panel b of Figure 11, it can be seen from the difference spectrum that the spectrum from the α[Zn]β[FeCO] in the presence of IHP resembles an intensity-reduced version of the deoxyHbA spectrum as inferred from the full spectrum shown in Figure 10. This intensity-reduced version of the deoxy T state spectrum is also seen both for the second intermediate formed when CO is added to sol−gel encapsulated deoxyHbA (*18*) and for the asymmetric cyanomet-deoxy hybrids of HbA (*74*). The generalized reduction in intensity has been attributed to a general weakening in both the T state interfacial contacts and the interhelical scaffolding that maintains the spacing between sets of helices (*18*, *72*, *74*, *75*, *77*, *78*).

In panel a of Figure 11, where the effector-free CO derivative is compared to deoxyHbA, it can be seen from a direct comparison and from the difference spectrum that for the hybrid the intensities of the three bands shown, 2xW18, W3, and Y8a, all show a decrease in intensity as in panel b. In addition, the Y8a band of the hybrid is shifted slightly to lower frequency as emphasized by the derivative-shaped feature in the difference spectrum. The Y8a shift is in the direction of the hybrid having the beginnings of an “R”-like signature with respect to this band; however, the shift is substantially less than the approximately 2 cm^{-1} shift that occurs when deoxyHbA is converted to COHbA as seen in panel d. The shift in Y8a to lower frequency in going from T to R structures is attributed primarily to the loss of the hydrogen bond between Asp β99 and Tyr α42 in the switch region of the $\alpha_1\beta_2$ interface (*69*, *71*). The most straightforward interpretation of the spectrum for the effector-free α[Zn]β[FeCO] is that it represents the next step in the sequence of conformational changes from deoxy T to liganded R in that there are still the loosened T state contacts but now we are seeing the onset of an R state interaction in the switch region of the $\alpha_1\beta_2$ interface.

In Figure 12 are shown the same spectra as in Figure 11, but in this instance the intensities of the Y8a and the W3 bands are each independently normalized with respect to the corresponding bands from deoxyHbA in order to facilitate the detection of the Y8a peak shifts and the changes in the low-frequency β37 sensitive shoulder of W3. It is clear that, for the effector-free and the plus IHP samples of α[Zn]β[FeCO], the W3 band behaves as anticipated from the above discussion. When intensity normalized, the W3 bands from the hybrid and deoxyHbA are very nearly superimposable. In contrast, the Y8a band from the hybrid shows clear evidence of shifts in frequency.

(D) UVRR Spectra of the CO-Saturated Derivatives of the α[Fe]β[Zn] Hybrid. The UVRR spectra from the α[FeCO]β[Zn] hybrid show similar features seen with the other hybrid but with some differences. Figure 13 compares the UVRR spectra of the hybrid to that of deoxyHbA as a function of added IHP ± L35. The intensity of the W3 and Y8a bands have been independently normalized as in Figure 12. It can be seen that, in the absence of effector, weak but clearly discernible R state signatures are seen for the Y8a band (shift to lower frequency) and the β37 shoulder of the W3 band (decreased intensity). The addition of IHP does not appreciably alter the spectrum. The combined addition of IHP and L35 reduces the difference in the Y8a band and induces

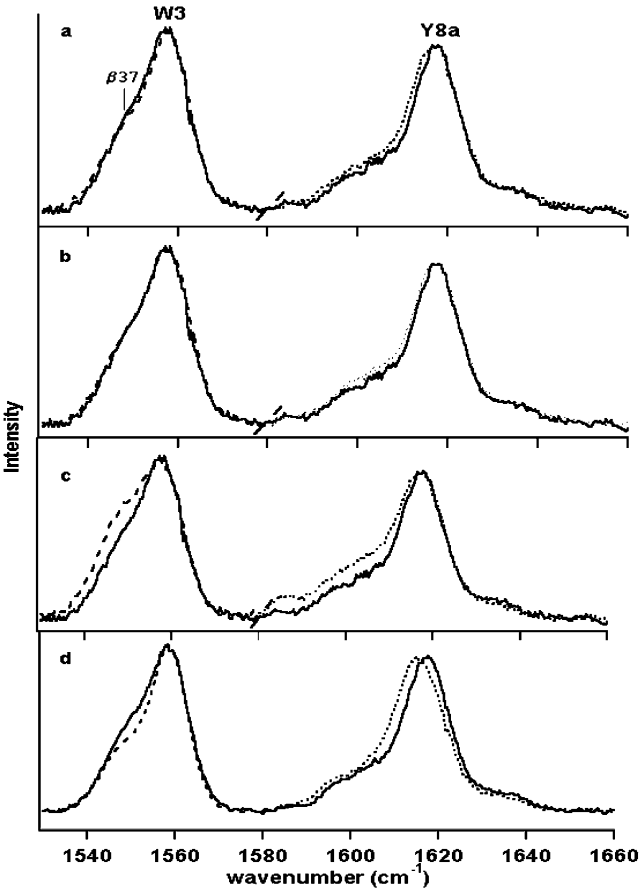

FIGURE 12: W3 and Y8a UVRR bands for solutions of α[Zn]β-[FeCO] with each of these two bands independently normalized to the same band from a deoxyHbA sample (solid line): (a) α[Zn]β-[FeCO]; (b) α[Zn]β[FeCO] + IHP; (c) α[Zn]β[FeCO] + IHP + L35; (d) COHbA (no normalization required).

the enhanced intensity in the β37 shoulder of the W3 band. Not shown is the behavior of 2xW18 band that, in contrast to the behavior seen for the previous hybrid, displays minimal intensity variation with addition of effectors. In all three cases (±IHP and IHP + L35) the intensity of this band is the same for the hybrid and for deoxyHbA. Within the context of the analysis presented above for the α[Zn]β[FeCO] samples, we interpret the UVRR spectra from the α[FeCO]β[Zn] samples as reflecting a continued but slight progression toward a more R-like species. The spectra shown in panel c of Figure 13 indicate that the α[FeCO]β[Zn] + IHP and L35 has a T state hinge region (as reflected in the behavior of the β37 shoulder of W3), but the small shift in the Y8a band signals the onset of R state properties for the switch region (vide supra). Thus the α[FeCO]β[Zn] sample with added effectors is similar conformationally to the effector-free sample of α[Zn]β-[FeCO].

Preliminary UVRR measurements (not shown) on sol−gel encapsulated FeZn hybrids indicate that the addition of CO to the encapsulated deoxy derivatives of the hybrids both with and without effectors results in half-liganded hybrids that exhibit spectra that are minimally changed with respect to the starting deoxy spectrum. This finding in conjunction with the solution phase UVRR results illustrates that there is a range of accessible conformations for the liganded Fe−Zn hybrids that appear to fall within the T state family and that isolation of these various T forms can be achieved using a balance between constraining elements (e.g., sol−gel, allosteric effectors) that limit conformational excursion from the stable deoxy T state structure and those factors, such as ligation, that favor T state destabilization.

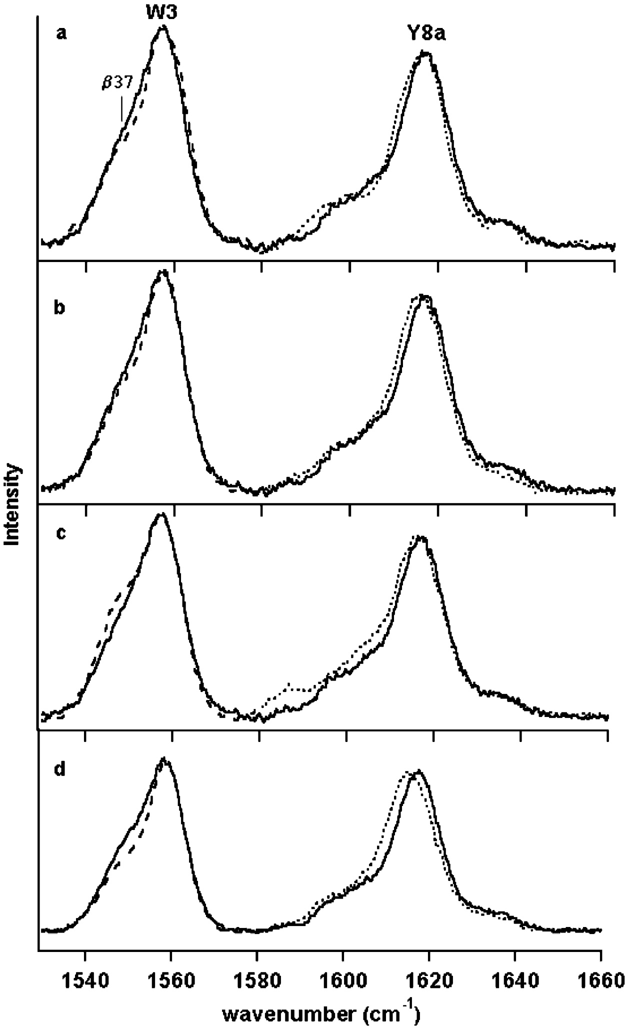

FIGURE 13: W3 and Y8a UVRR bands for solutions of α[FeCO]β-[Zn] with each of these two bands independently normalized to the same band from a deoxyHbA sample (solid line): (a) α-[FeCO]β[Zn]; (b) α[FeCO]β[Zn] + IHP; (c) α[FeCO]β[Zn] + IHP + L35; (d) COHbA (no normalization required).

Previous studies have also identified species that exhibit UVRR spectra with reduced intensity. Typically, samples exhibiting such behavior are species that are likely to be near or at the transition state for the R−T quaternary transition. Both R and T state species having this property have been identified. Deoxy R state species observed either in time-resolved photolysis experiments (*72*, *79*), in Hb mutants (*57*), or in chemically modified Hbs (*75*) exhibit the R signatures with respect to peak positions in the UVRR spectrum but also exhibit a general decrease in peak intensity across the spectrum. These same low-intensity R state UVRR spectra were observed for the half-liganded derivatives of Fe−Co hybrids (*72*) and triply liganded R state species (*74*). Similarly, a liganded T state form of HbA, trapped within a porous sol−gel matrix, exhibited the T signature in the UVRR spectrum but, as with the deoxy R species, there was a decrease in peak intensity across the spectrum (*18*). A similar T state spectrum was reported for asymmetric deoxy-cyanomet hybrids of HbA (*74*). In the present study both R and T state-like UVRR spectra with reduced intensity are observed for the liganded hybrids.

The above pattern of intensity reduction in the UVRR spectra of hemoglobins has been attributed to a weakening of the interhelical hydrogen bonds and salt bridges that act as scaffolding for the stable and compact end-point structures such as the deoxy T and liganded R conformations (*57*, *75*). The process of ligand binding and ligand dissociation weakens these interactions for the T and R state structures, respectively. Thus both the liganded T and deoxy R are structures in which the scaffolding is loosened. The observation that the UVRR spectra of liganded Fe−Zn hybrids can easily be made to exhibit either R, T, or mixed state signatures by varying the solution conditions suggests that, under conditions where the scaffolding is loosened, there is a reduction in the energetic cost of switching between quaternary states. This pattern suggests that under these conditions there has been a disengaging of the constraints within the $\alpha_1\beta_2$ interface that stabilize the usual end-point structures for HbA. If this hypothesis is borne out, it would support the concept that conformations with the weakened or loosened scaffolding are well suited for the role of R−T transition states. Furthermore, the UVRR and the VRR together indicate that, under conditions where the T state interfacial constraints are loosened, proximal strain can be drastically reduced as reflected in the increased frequency of ν(Fe−His) for the half-liganded photoproducts of the FeZn hybrids.

DISCUSSION

Functional Properties of FeZn Hybrids: Kinetics of CO Combination with Unliganded Hybrids. The rate constants for the combination of CO with the Fe−Zn hybrids of HbA are consistent with the initial rates of CO combination with HbA. At pH 7 in the absence of IHP or L35, the latter rate constant is approximately 0.1 $\mu\mathrm{M}^{-1}\ \mathrm{s}^{-1}$ while in the presence of IHP it is 0.06 $\mu\mathrm{M}^{-1}\ \mathrm{s}^{-1}$. These values are similar to the averages of the values for l'_1 for the two FeZn hybrids in the absence and presence of IHP, respectively. Although the reaction of CO with HbA is an accelerating process, with the reaction rate increasing as much as a factor of 4 as the reaction proceeds, no similar acceleration is observed with the FeZn hybrids. On the contrary, in the absence of organic phosphates the kinetic properties of both FeZn hybrids indicate the presence of a small, but reproducible, negative interaction between the two heme-containing subunits. The kinetics are decelerating and are best fitted not by a sum of exponential functions but by a sequential reaction mechanism. The indication is that the sites that bind CO more slowly are not present initially but form as a result of binding a CO molecule at one heme site on the Fe−Zn hybrid hemoglobin molecule. The addition of IHP to α[Fe]β[Zn] reduces l'_1 by about 25% without affecting l'_2, eliminating kinetic heterogeneity. Addition of IHP has a much larger effect on the rate of CO combination to α[Zn]β[Fe]. Both l'_1 and l'_2 are reduced to approximately 40% of their values in its absence. In this case kinetic heterogeneity is maintained. The kinetic properties of the hybrids are those expected of the deoxygenated T conformational state of the Hb molecule. The data in Table 1 are in close agreement with the kinetic results of Blough et al. (*4*, *80*), with the exception that those authors did not report the slight deceleration of the CO combination reactions described in the present study.

Table 4: Oxygen Affinities and Hill Coefficients of Hemoglobin Crystals

species	p_{50} (a)[a]	p_{50} (c)[a]	Hill *n* (a)[a]	Hill *n* (c)[a]
HbA[d]	135	133	1.00	1.01
HbA + IHP[d]	136	132	0.94	0.95
HbA+ BZF[d]	133	128	0.96	0.97
β chains in HbA[d]	200			
α chains in HbA[d]	79			
α[Ni]β[Fe][e]	123	102 (*b*)[b]	0.87	0.93
α[Fe]β[Ni][f]	95 (*b*)[c]	87	0.96	0.90
α[Zn]β[Fe]	154	152	1.13	1.08
α[Fe]β[Zn]	81	81	1.08	1.10

[a] (a) and (c) refer to measurements carried out with light polarized parallel to these principle optical axes of the crystal. [b] With crystals of the α[Ni]β[Fe] hybrid, measurements can be made only along the *a* and *b* optical axes. [c] With crystals of the α[Ni]β[Fe] hybrid, measurements can be made only along the *b* and *c* optical axes. [d] Mozzarelli et al. (*81*). [e] Betatti et al. (*82*). [f] Bruno et al. (*7*)

Equilibrium of Oxygen Binding to FeZn Hybrids in Solution. As shown in Table 2, the affinities of the two FeZn hybrids of HbA are also consistent with the properties expected of the deoxygenated T conformational state of HbA. No cooperativity in ligand binding is observed. The addition of IHP results in a marked reduction in the oxygen affinities of both hybrids, consistent with earlier reports of the effects of this allosteric effector on K_1 of HbA. However, the IHP effect is significantly greater for the β subunit than for the α subunit.

In their studies of mixed-metal hybrids of HbA Miyazaki et al. (*8*) also measured equilibria of oxygen binding to α[Zn]β[Fe] and α[Fe]β[Zn] hybrids. Although their measurements were not carried out under the same conditions used in the present study, the oxygen affinities they reported are, in general, consistent with our data. However, they report greater cooperativity than indicated by our results: $n = 1.1$ in most experiments at pH 6.5 or 7.4. Since the hemoglobin concentration used in their study was 60 μM in heme equivalents, considerably lower than used in the present work, the observed cooperativity might be due in part to some dissociation of the diliganded protein into αβ dimers which have higher oxygen affinity than the T state tetramer. The possible role of dissociation into αβ dimers is consistent with the still higher Hill coefficients reported at pH 8.5 where such dissociation is expected to be greater. In general, the equilibrium and kinetic properties of the Fe−Zn hybrids reported here correlate well with those previously reported for similar hybrids prepared in other laboratories by different procedures.

Extreme T State Behavior Observed in the Oxygen Binding to Crystals of the Fe−Zn Hybrids. The affinities of α and β hemes in crystals of Fe−Zn hybrids are compared with those calculated for Hb A crystals in either the absence or presence of IHP or bezafibrate and with those determined for Fe−Ni hybrid crystals in the presence of IHP (Table 4). The values of p_{50} estimated for the α subunit are in close agreement, ranging from 79 to 95 Torr, whereas the values of p_{50} for the β subunit vary from 102 to 200 Torr. Recent calculations by Mozzarelli et al. led to an estimate of a 2.5-fold difference (*81*). The experimental determinations of α and β affinities, using Fe−Ni metal hybrid crystals of space group $P2_1$, indicate that the average α/β affinity ratio is 1.2 (*7*, *82*). These same oxygen binding measurements have also evidenced the existence of a 1.3-fold difference in oxygen affinity between α_1 and α_2 and between β_1 and β_2 in these crystals (*82*), due to asymmetric subunit interactions within the crystal packing. This finding is in agreement with structural evidence indicating different occupancy of oxygen molecules within a fully liganded hemoglobin (*83*). However, in the present study an α/β affinity ratio of 1.8 is found, and the oxygen affinities measured along the two polarization directions are much more similar than in Ni hybrids, suggesting negligible difference between the affinities of α_1 and α_2 hemes and β_1 and β_2 hemes.

In general, the oxygen affinities of T state crystals of HbA approximate K_1, the oxygen affinity of the deoxygenated T state in solution, in the presence of IHP. This finding has been interpreted as being due to the stabilization in the crystal of a very low oxygen affinity substate of the quaternary T structure of hemoglobin. Such a low-affinity substate of hemoglobin becomes fully populated in solution when allosteric effectors are present (*24*). The Fe−Zn hybrids are seen to follow the same pattern. The measurements of oxygen affinity of the crystalline hybrids were carried out at 15 °C while those of affinities in solution were at 20 °C. Since a 10 deg increase in temperature decreases the oxygen affinity of HbA by a factor of 2 (*84*), division of the dissociation constants measured at 20 °C by a factor of 1.4 permits a direct comparison with the crystal measurements. For the α subunits in the α[Fe]β[Zn] hybrid, the corrected p_{50} in solution in the presence of IHP is 91 Torr, which compares well with 81 Torr for the crystals of this hybrid. The corrected p_{50} for the α[Zn]β[Fe] hybrid is 129 Torr, which is roughly 20% less than p_{50} for the crystal. The two equilibrium constants yield an α−β affinity ratio in solution in the presence of IHP of 1.4. In the absence of IHP, the corrected p_{50} values for α[Fe] and β[Fe] subunits are both 47 Torr, indicating significantly greater affinities than found for the crystals. It is remarkable that the affinity of HbA crystals is the same as the low oxygen affinity T state isolated in Hb gels (*41*). Finally, the Hill coefficients of metal hybrids in the crystal are always very close to unity (Table 4). This finding is in agreement with findings in solution in the present study and elsewhere (*8*, *85*).

Functional Properties of [FeCO]$_2$[Zn]$_2$ Hybrids: CO Recombination. Ligand binding parameters associated with the first ligation step for the deoxy derivatives of the hybrids are unambiguous in that they are readily attributed to the properties of an initial deoxy T state population. The absence both of cooperativity in binding equilibria and of acceleration in reaction kinetics is consistent with the second step in the saturation process involving only the low-affinity T state as well. However, these data cannot define with precision the properties of the diliganded hybrids. In the framework of the traditional two-state model (*86*), the presence of 20% R state in the population of diliganded tetramers would only raise the affinity of the second binding reaction by 20% and might not be detected, particularly if there is negative cooperativity in ligand binding to like subunits in the low-affinity T state as concluded by Ackers and others (*87*, *88*).

The use of CO as a ligand ensures a maximally liganded population. Geminate recombination of CO will reflect the properties of the starting photodissociated population. The slower bimolecular rebinding will typically contain contributions from the initial distribution of structures as well as from populations that have undergone relaxation of the initial quaternary and tertiary conformations. It has been shown that, under appropriate conditions, sol−gel encapsulation will slow or eliminate conformational relaxation (in particular, the R → T transition) on the time scale of the rebinding (*15*, *17*, *63*). Under these conditions, it is anticipated that the full range of rebinding phenomena will reflect the starting equilibrium-liganded population.

The kinetic traces for both hybrids at pH 6.5 in the presence of both IHP and L35 are consistent with an initial population that is overwhelmingly T state. The geminate yield is at a minimum. The slower bimolecular phase is characteristic of the slow T state combination rate observed in the rapid mix experiments, and there is no indication of a separate kinetic phase that corresponds to the R state bimolecular reaction. This conclusion is supported by nearly identical kinetic traces of the corresponding samples encapsulated in the sol−gel where relaxation is reduced or eliminated. Furthermore, nearly the same traces are obtained when the fully deoxy hybrids are initially encapsulated and then exposed to CO after the gel has aged. Under those conditions, the initial quaternary/tertiary conformation of the deoxy derivatives is “locked in” and retained after ligation.

In the absence of effectors, the pH 6.5 solution phase samples of the two hybrids both exhibit a distinct geminate phase that is intermediate between what is observed for COHbA and what is observed for the hybrids in the presence of both IHP and L35. The α Zn hybrid exhibits a lower geminate yield (∼30%) than the β Zn hybrid (∼50%). The geminate yield for COHbA under these conditions is ∼65%. The intermediate values for the geminate yield might suggest that the starting population for the hybrids is a simple mixture of liganded R (with a geminate yield of 65%) and liganded T (with a nearly zero geminate yield) species. Several observations argue against this hypothesis.

For both hybrids, there is no evidence of a distinct bimolecular phase corresponding to the R state solvent phase seen for COHbA. The absence of this phase is not necessarily a feature associated with half-liganded species since both the normal R state geminate phase (with 65% geminate yield) and an R state bimolecular phase are observed for α[Co]β[FeCO]. In contrast, the bimolecular phase for both effector-free samples of Fe−Zn hybrids has the appearance of a T state population with no clear R state fast phase. However, the α[Zn]β[FeCO] hybrid does exhibit a bimolecular recombination phase with significant heterogeneity. Part of the process takes place between 10^{-5} and 10^{-3} s where rebinding to the R state normally occurs. However, the typical transition between R state and T state phases is not present. These observations argue against there being a large starting population of a liganded R state species similar to that which occurs for COHbA or α[Co]β[FeCO]. This point is especially true of the α[FeCO]β[Zn] sample where the geminate yield is close to that observed for COHbA, but with bimolecular rebinding that is quite homogeneous and T-like.

A second argument against the hypothesis that a simple mixture of liganded R and T species can characterize the starting hybrid population comes from the sol−gel results. Since the sol−gel eliminates the R to T transition for photodissociated COHbA, it is anticipated that if there were a substantial R state population that were undergoing rapid relaxation, stopping the relaxation via sol−gel encapsulation would result in the appearance of the R state bimolecular recombination. Contrary to this expectation, sol−gel encapsulation of α[Zn]β[FeCO] in the absence of IHP results in a relatively homogeneous bimolecular kinetic phase with no significant reaction occurring in the 10^{-5}−10^{-3} s time interval. On the other hand, encapsulation of the α[FeCO]β-[Zn] hybrid under the same conditions results in a very heterogeneous bimolecular reaction, a large fraction of which occurs between 10^{-5} and 10^{-3} s, whereas in solution these same conditions result in no significant reaction in this time interval. However, when deoxygenated α[Fe]β[Zn] is encapsulated and then made CO, the bimolecular phase remains heterogeneous, although somewhat less so, with significant reaction in the 10^{-5}−10^{-3} s interval. These observations argue against the possibility that the absence of the R state recombination phase in solution originates from a rapid and complete relaxation of a starting photodissociated R state population to a full T state population prior to the onset of the solvent phase bimolecular recombination process.

Conformational Properties of Solution Phase Fe−Zn Hybrids. The VRR and UVRR spectra of the deoxy Fe−Zn hybrids are both entirely consistent with conformations that are essentially identical to the equilibrium deoxy T state structure observed for HbA. This result is not unexpected given the solution phase CO on rates and the oxygen binding properties of the deoxy hybrid crystals. As observed for several other T state deoxy Fe−metal hybrids, the frequency of ν(Fe−His) for the α[Fe] is substantially less than for the β[Fe]. The lower frequency is an indication of the increased proximal strain associated with the unliganded α subunit of the T state tetramer.

Conformational evaluation of the half-liganded hybrids is not clear-cut. The UVRR and VRR show a clear progression for both half-liganded hybrids with respect to added effectors. In the presence of both IHP and L35, the frequency of ν(Fe−His) for the iron heme photoproduct is in the 220−223 cm^{-1} range. This range is similar to values obtained from liganded Hbs that are stabilized in the T state (*51*, *52*, *89*). These include NOHbA + IHP (*11*), COHb (Kansas) + IHP (*51*), and sol−gel encapsulated deoxyHbA to which CO is added (*20*). The liganded T state assignment for the half-liganded FeZn hybrids in the presence of IHP and L35 is supported by the T state features seen in the UVRR indicative of the $\alpha_1\beta_2$ interface having T state contacts. In the progression from samples having both effectors to just IHP to no added effectors, the photoproduct frequency of ν(Fe−His) for the half-liganded hybrids increases into a regime that is traditionally viewed as being reflective of liganded R state species. For the Fe−Zn hybrids neither the UVRR nor the kinetic traces support the presence of a sizable population of a liganded R state (similar to the R state accessed by COHbA). In contrast, the photoproduct of α[Co]β[FeCO] also has a high frequency for ν(Fe−His) that is typical of an R state photoproduct, but in this case rebinding kinetics are fully consistent with a liganded R state population.

The FeZn hybrid data are most consistent with either of two scenarios. The first scenario is that the conformational populations for each sample are largely homogeneous. The progression for the hybrids from the deoxy derivatives to half-liganded hybrids with both effectors to half-liganded hybrids with IHP to half-liganded hybrids with no effectors would therefore reflect a progression of T state conformations and functionalities. The progression would start from the most stable and compact T state conformations with strong T state contacts (salt bridges and hydrogen bonds contributing to the stability of the T quaternary structure) and high proximal strain at the α subunit upon ligand binding and progress to conformations with weakened T state contacts, looser scaffolding, and diminished proximal strain. The second scenario is similar but has the added element that, toward the end of the progression, the population becomes inhomogeneous with both R and T state species contributing. In this case, both the T and R state species contributing are not likely to be the equilibrium T and R species associated with the deoxy and fully liganded end-point conformations of HbA.

Support for these scenarios comes from several sources. A comparison of effector-dependent oxygen binding properties of HbA in crystals, sol−gel matrices, and solution reveals a range of T state functionalities consistent with low- and high-affinity T conformations (*41*, *90*).

Recently, Yonetani and co-workers (*91*) interpreted their results to show that both the T and R quaternary states can accommodate a wide range of effector-dependent oxygen affinities, implying a wide range of accessible tertiary conformations for each quaternary state. Nevertheless, for each set of solution conditions there is a clear-cut ligation-induced T to R transition (with a solution-dependent increase in oxygen affinity). When comparing oxygen affinity as a function of solution conditions, the range of oxygen affinities for R and T has regions of overlap. As a result the R state under one set of solution conditions can have a lower affinity than T state species stabilized under different solution conditions (e.g., R state in the presence of a combination of effectors versus T state in the absence of effectors). Furthermore, there are solution conditions where the T and R states have similar oxygen affinity (with R having slightly higher affinity). These conditions are also associated with decreased stability of both quaternary states. If the liganded hybrid data in the present study reflect an inhomogeneous population, it is likely that we are accessing regimes where there are conformational substates of R and T having similar reactivity and stability that are easily interconverted through manipulation of solution conditions (due to low-energy barriers), as would be expected for species having transition state properties.

Relationship between Conformation and Ligand Reactivity. The CO combination rates for the Fe−Zn hybrids and the oxygen binding properties of the deoxy crystals of the Fe−Zn hybrids are all consistent with the known ligand binding properties of the lowest affinity form of the T state. In contrast, the effector-dependent functional properties of the half-liganded hybrids span a broad range of reactivities. As noted earlier, the effector-dependent kinetic traces for the rebinding of CO to the photodissociated hybrids cannot be explained using the standard R and T state properties associated with HbA. The geminate yield follows the same progression as the Raman results in that samples exhibiting higher frequencies for ν(Fe−His) exhibit higher geminate yields. This progression is also reflected in the UVRR where the lowest geminate yields are associated with the samples with UVRR spectra most closely resembling that of the deoxyHbA and the highest geminate yields are associated with samples having spectra indicative of either a "loosened" T state conformation or a mix of the loosened T species with a small population having an R state conformation. The increased geminate yield of the loosened T state species is consistent with an increased ligand affinity.

All of the presented kinetic traces show either of two patterns for the bimolecular rebinding. In one case there is only the single slow phase that is associated with conventional T state populations. In the other case, there is still the distinct slow T state phase, but there is also a nearly continuous distribution of rebinding rates that extends from the traditional R state regime into the T state regime. An implication of the present work is that the loosened T state constraints give rise to a distribution of barrier heights controlling iron−ligand bond formation. For the α hemes this distribution is likely to arise from a distribution in the proximal strain related to the loosening of the hinge region of the $\alpha_1\beta_2$ interface. A distribution in the positioning of Val E11 in the β subunits is likely to be a major contributor for the distribution of barrier heights for that subunit. Use of Mb mutants has clearly demonstrated the potential role of the E11 residue in blocking or opening ligand access to the heme iron. It is interesting to note that Yonetani (*91*) reported that the distribution of functionally distinct forms of HbA was paralleled by a distribution of tertiary conformations as reflected in the NMR signal from Val E11.

Thus the kinetic heterogeneity could be accounted for by either a distribution of intermediate tertiary conformations or a distinct intermediate tertiary/quaternary conformation that contains a slowly interconverting distribution of accessible conformational substates with differing positions for loosened gate keeper residues such as E11 and B10 as well as residues impacting proximal strain (e.g., β37 and α140). For these intermediate species (vis à vis deoxy T and liganded R HbA), the proposed broad distribution of positions for these residues and the rate at which they interconvert (temperature and viscosity dependent) should determine the distribution of rebinding rates.

Spectroscopic Signature of the High- and Low-Affinity T State Species. Evidence for high and low oxygen affinity forms of the T state HbA has emerged from ligand binding properties of HbA in solution phase in the presence of allosteric effectors and of HbA in crystals (*14*, *16*, *81*, *92*) and in sol−gel matrices (*16*, *41*, *90*). The conformational basis for these states is still unclear. The functional and spectroscopic studies on the Fe−Zn hybrids under a diverse range of conditions (solution, crystal, sol−gel, ±effectors) provided an opportunity to systematically generate and probe a range of T state properties. The results support the idea that the variation in T state properties originates from the extent to which the initial deoxy T state conformation evolves upon ligand binding. Factors such as sol−gel encapsulation, crystallization, and allosteric effectors which limit the diligation-induced conformational evolution toward the loosened, less constrained T state favor the low-affinity forms of the T state.

Subunit-Specific Differences in the Mechanism of Ligation-Induced Destabilization of the Deoxy T State Conformation. The present study as well as previous studies shows that having cobalt in the α subunits provides much more of a T state destabilization than the corresponding substitution in the β subunits (*93*, *94*). Additional studies (*14*) on a variety of hybrids provided evidence that the metal-specific displacement of the F helix in the α subunits was a significant factor in the destabilization of the T state. Thus the destabilization effect of Co in the α subunits is explainable on the basis of it being situated closer to the heme plane than either high-spin ferrous iron or Zn. Thus the α Co behaves almost like a liganded iron, and as a consequence, ligand binding to the ferrous-containing β subunits accesses the liganded R state more readily than for the corresponding α Zn hybrid. It is also clear that for the β subunit it is not the metal or F helix displacement per se that is the destabilizing parameter; rather it is the actual presence of a ligand at the iron binding site in the β subunit that is required for β heme-derived destabilization of the T state. This point is reflected in the retention of the T state kinetic and spectroscopic patterns for the α[FeCO]β[Co] hybrid as well as the geminate yield differences between the two Fe/Zn hybrids and the sensitivity of the kinetics and spectra of the two different half-liganded hybrids to added effectors.

The UVRR supports this assessment of the subunit-specific role of ligand binding in the destabilization of the T state. The hinge region of the αβ interface has been shown to be the major determinant of T state stability. Furthermore, studies on β37 mutants of HbA show that the status/stability of the hinge region directly impacts the degree of proximal strain at the heme of the α subunit. The present study directly demonstrates that ligand binding to α subunits is significantly more effective in destabilizing the T state hinge than is ligand binding to the β subunits. This result supports the lever arm model in which ligation in the α subunit is directly coupled to the hinge (β37W) through the movement of the α subunit iron directly loosening the packing of the β37W side chain by shifting the position of the α140Y side chain. In the deoxy T state, the α140Y side chain packs up against the indole ring of β37W, thus stabilizing the T state hinge configuration. The ligation-induced movement of the α140Y side chain out of its constrained and relatively hydrophobic deoxy T state site is likely a source of the T state ligation-induced intensity decrease observed for tyrosine bands in UVRR spectra.

SUMMARY

The presented results show that the deoxy derivatives of the FeZn hybrids of HbA are conformationally and functionally similar to that of deoxyHbA. In contrast, there is an effector-dependent distribution of functional and conformational properties associated with the diliganded (CO) derivative of the hybrids. This range of effector-dependent functional and conformational properties of the diliganded hybrids is most consistent with a progression of tertiary conformations within the overall T quaternary state. These extend from the equilibrium deoxy T state conformation to conformations that reflect considerable destabilization of the T state constraints and thus are likely transition state species. The properties of the hybrids observed in solution, in the crystal, and in sol−gel matrices support the concept that ligand binding properties within the T state result from a balance of forces, some of which favor retention of the initial low-affinity deoxy T state conformation (e.g., crystal, sol−gel, effectors) and those (diligation) that favor a "loosening" of T state constraints. Thus the results are consistent with considerable plasticity of tertiary structure within the constraints of the T quaternary structure. It is also apparent that as the tertiary structure progresses from the crystallographically well-defined deoxy T state low-affinity end point, the spectroscopic signatures of quaternary structure become progressively more ambiguous.

REFERENCES

1. Perutz, M. F., Wilkinson, A. J., Paoli, M., and Dodson, G. G. (1998) *Annu. Rev. Biophys. Biomol. Struct. 27*, 1−34.
2. Mueser, T. C., Rogers, P. H., and Arnone, A. (2000) *Biochemistry 39*, 15353−15364.
3. Unzai, S., Hori, H., Miyazaki, G., Shibayama, N., and Morimoto, H. (1996) *J. Biol. Chem. 271*, 12451−12456.
4. Blough, N. V., and Hoffman, B. M. (1984) *Biochemistry 23*, 2875−2882.
5. Shibayama, N., Imai, K., Morimoto, H., and Saigo, S. (1995) *Biochemistry 34*, 4773−4780.
6. Chavez, M. D., Courtney, S. H., Chance, M. R., Kiula, D., Nocek, J., Hoffman, B. M., Friedman, J. M., and Ondrias, M. R. (1990) *Biochemistry 29*, 4844−4852.
7. Bruno, S., Bettati, S., Manfredini, M., Mozzarelli, A., Bolognesi, M., Deriu, D., Rosano, C., Tsuneshige, A., Yonetani, T., and Henry, E. R. (2000) *Protein Sci. 9*, 683−692.
8. Miyazaki, G., Morimoto, H., Yun, K. M., Park, S. Y., Nakagawa, A., Minagawa, H., and Shibayama, N. (1999) *J. Mol. Biol. 292*, 1121−1136.
9. Shibayama, N., Yonetani, T., Regan, R. M., and Gibson, Q. H. (1995) *Biochemistry 34*, 14658−14667.
10. Sudhakar, K., Laberge, M., Tsuneshige, A., and Vanderkooi, J. M. (1998) *Biochemistry 37*, 7177−7184.
11. Friedman, J. M., Scott, T. W., Stepnoski, R. A., Ikeda-Saito, M., and Yonetani, T. (1983) *J. Biol. Chem. 258*, 10564−10572.
12. Hofrichter, J., Henry, E. R., Sommer, J. H., Deutsch, R., Ikeda-Saito, M., Yonetani, T., and Eaton, W. A. (1985) *Biochemistry 24*, 2667−2679.
13. Ondrias, M. R., Rousseau, D. L., Kitagawa, T., Ikeda-Saito, M., Inubushi, T., and Yonetani, T. (1982) *J. Biol. Chem. 257*, 8766−8770.
14. Fujii, M., Hori, H., Miyazaki, G., Morimoto, H., and Yonetani, T. (1993) *J. Biol. Chem. 268*, 15386−15393.
15. Shibayama, N., and Saigo, S. (1995) *J. Mol. Biol. 251*, 203−209.
16. Bettati, S., and Mozzarelli, A. (1997) *J. Biol. Chem. 272*, 32050−32055.
17. Das, T. K., Khan, I., Rousseau, D. L., and Friedman, J. M. (1999) *Biospectroscopy 5*(S), 54−70.
18. Juszczak, L. J., and Friedman, J. M. (1999) *J. Biol. Chem. 274*, 30357−30360.
19. Khan, I., Shannon, C. F., Dantsker, D., Friedman, A. J., Perez-Gonzalez-de-Apodaca, J., and Friedman, J. M. (2000) *Biochemistry 39*, 16099−16109.
20. Samuni, U., Dantsker, D., Khan, I., Friedman, A. J., Peterson, E., and Friedman, J. M. (2002) *J. Biol. Chem. 25*, 25.
21. Arnone, A., and Perutz, M. F. (1974) *Nature 249*, 34−36.
22. Wireko, F. C., Kellogg, G. E., and Abraham, D. J. (1991) *J. Med. Chem. 34*, 758−767.
23. Perutz, M. F., and Poyart, C. (1983) *Lancet 2*, 881−882.
24. Lalezari, I., Lalezari, P., Poyart, C., Marden, M., Kister, J., Bohn, B., Fermi, G., and Perutz, M. F. (1990) *Biochemistry 29*, 1515−1523.
25. Rossi-Fanelli, A., Antonini, E., and Caputo, A. (1958) *Biochim. Biophys. Acta 30*, 608.
26. Hui, H. L., Kavanaugh, J. S., Doyle, M. L., Wierzba, A., Rogers, P. H., Arnone, A., Holt, J. M., Ackers, G. K., and Noble, R. W. (1999) *Biochemistry 38*, 1040−1049.
27. Clegg, J. B., Naughton, M. A., and Weatherall, D. J. (1965) *Nature 207*, 945−947.
28. Clegg, J. B., Naughton, M. A., and Weatherball, D. J. (1966) *J. Mol. Biol. 19*, 91−108.
29. Noble, R. W., Hui, H. L., Kwiatkowski, L. D., Paily, P., DeYoung, A., Wierzba, A., Colby, J. E., Bruno, S., and Mozzarelli, A. (2001) *Biochemistry 40*, 12357−12368.
30. Gibson, Q. H. (1959) *Biochem. J. 91*, 161−170.
31. Doyle, M. L., Lew, G., De Young, A., Kwiatkowski, L., Wierzba, A., Noble, R. W., and Ackers, G. K. (1992) *Biochemistry 31*, 8629−8639.
32. Allen, D. W., Guthe, K. F., and Wyman, J. (1950) *J. Biol. Chem. 187*, 393−410.
33. Nagel, R. L., Wittenberg, J. B., and Ranney, H. M. (1965) *Biochim. Biophys. Acta 100*, 286−289.
34. Hayashi, A., Suzuki, T., and Shin, M. (1973) *Biochim. Biophys. Acta 310*, 309−316.
35. Rivetti, C., Mozzarelli, A., Rossi, G. L., Kwiatkowski, L. D., Wierzba, A. M., and Noble, R. W. (1993) *Biochemistry 32*, 6411−6418.
36. Bettati, S., Kwiatkowski, L. D., Kavanaugh, J. S., Mozzarelli, A., Arnone, A., Rossi, G. L., and Noble, R. W. (1997) *J. Biol. Chem. 272*, 33077−33084.
37. Dvorak, J. A., and Stotler, W. F. (1971) *Exp. Cell Res. 68*, 144−148.
38. Rivetti, C., Mozzarelli, A., Rossi, G. L., Henry, E. R., and Eaton, W. A. (1993) *Biochemistry 32*, 2888−2906.
39. Ellerby, L. M., Nishida, C. R., Nishida, F., Yamanaka, S. A., Dunn, B., Valentine, J. S., and Zink, J. I. (1992) *Science 255*, 1113−1115.
40. Abbruzetti, S., Viappiani, C., Bruno, S., Bettati, S., Bonaccio., M., and Mozzarelli, A. (2001) *J. Nanosci. Nanotechnol. 1*, 407−413.
41. Bruno, S., Bonaccio, M., Bettati, S., Rivetti, C., Viappiani, C., Abbruzzetti, S., and Mozzarelli, A. (2001) *Protein Sci. 10*, 2401−2407.
42. Dantsker, D., Samuni, U., Friedman, A. J., Yang, M., Ray, A., and Friedman, J. M. (2002) *J. Mol. Biol. 13*, 239−251.
43. Austin, R. H., Beeson, K. W., Eisenstein, L., Frauenfelder, H., and Gunsalus, I. C. (1975) *Biochemistry 14*, 5355−5373.
44. Doster, W., Kleinert, T., Post, F., and Settles, M. (1993) in *Protein−Solvent Interactions* (Gregory, R. B., Ed.) Marcel Dekker, New York.
45. Samuni, U., Navati, M. S., Juszczak, L. J., Dantsker, D., Yang, M., and Friedman, J. M. (2000) *J. Phys. Chem. B 104*, 10802−10813.
46. Alpert, B., El Mohsni, S., Lindqvist, L., and Tfibel, F. (1979) *Chem. Phys. Lett. 64*, 11−16.
47. Duddell, D., Morris, R., and Richards, J. (1979) *J. Chem. Soc., Chem. Commun. 2*, 75−76.
48. Friedman, J. M., and Lyons, K. B. (1980) *Nature 284*, 570−572.
49. Antonini, E., and Brunori, M. (1971) *Hemoglobins and Myoglobins in their Reactions with Ligands*, American Elsevier Co., New York.
50. Abbruzetti, S., Viappiani, C., Bruno, S., and Mozzarelli, A. (2001) *Chem. Phys. Lett. 346*, 430−436.
51. Friedman, J. M., Rousseau, D. L., Ondrias, M. R., and Stepnoski, R. A. (1982) *Science 218*, 1244−1246.
52. Friedman, J. M. (1985) *Science 228*, 1273−1280.
53. Findsen, E. W., Friedman, J. M., Ondrias, M. R., and Simon, S. R. (1985) *Science 229*, 661−665.
54. Friedman, J. M. (1994) *Methods Enzymol. 232*, 205−231.
55. Rousseau, D. L., and Friedman, J. M. (1988) in *Biological Applications of Raman Spectroscopy* (Spiro, T. G., Ed.) pp 133−215, John Wiley & Sons, New York.
56. Kitagawa, T. (1988) in *Biological Application of Raman Spectroscopy* (Spiro, T. G., Ed.) pp 97−131, John Wiley & Sons, New York.
57. Huang, J., Juszczak, L. J., Peterson, E. S., Shannon, C. F., Yang, M., Huang, S., Vidugiris, G. V., and Friedman, J. M. (1999) *Biochemistry 38*, 4514−4525.
58. Hu, X., Rodgers, K. R., Mukerji, I., and Spiro, T. G. (1999) *Biochemistry 38*, 3462−3467.
59. Peterson, E. S., and Friedman, J. M. (1998) *Biochemistry 37*, 4346−4357.
60. Khan, I., Dantsker, D., Samuni, U., Friedman, A. J., Bonaventura, C., Manjula, B., Acharya, S. A., and Friedman, J. M. (2001) *Biochemistry 40*, 7581−7592.
61. Friedman, J. M., Scott, T. W., Fisanick, G. J., Simon, S. R., Findsen, E. W., Ondrias, M. R., and Macdonald, V. W. (1985) *Science 229*, 187−190.
62. Scott, T. W., and Friedman, J. M. (1984) *J. Am. Chem. Soc. 106*, 5677−5687.
63. Shibayama, N. (1999) *J. Mol. Biol. 285*, 1383−1388.
64. Podstawka, E., Rajani, C., Kincaid, J. R., and Proniewicz, L. M. (2000) *Biopolymers 57*, 201−207.
65. Zhao, X., Chen, R., Raj, V., and Spiro, T. G. (2001) *Biopolymers 62*, 158−162.
66. Su, C., Park, Y. D., Liu, G., and Spiro, T. G. (1989) *J. Am. Chem. Soc. 111*, 3457−3459.

67. Rodgers, K., Su, S., Subramaniam, S., and Spiro, T. (1992) *J. Am. Chem. Soc. 114*, 3697−3709.
68. Nagai, M., Kaminaka, S., Ohba, Y., Nagai, Y., Mizutani, Y., and Kitagawa, T. (1995) *J. Biol. Chem. 270*, 1636−1642.
69. Huang, S., Peterson, E. S., Ho, C., and Friedman, J. M. (1997) *Biochemistry 36*, 6197−6206.
70. Nagai, M., Wajcman, H., Lahary, A., Nakatsukasa, T., Nagatomo, S., and Kitagawa, T. (1999) *Biochemistry 38*, 1243−1251.
71. Wang, D., Zhao, X., and Spiro, T. G. (2000) *J. Phys. Chem. 104*, 4149−4152.
72. Rodgers, K. R., and Spiro, T. G. (1994) *Science 265*, 1697−1699.
73. Mukerji, I., and Spiro, T. G. (1994) *Biochemistry 33*, 13132−13139.
74. Jayaraman, V., and Spiro, T. G. (1995) *Biochemistry 34*, 4511−4515.
75. Wang, D., and Spiro, T. G. (1998) *Biochemistry 37*, 9940−9951.
76. Wang, D., Zhao, X., Shen, T.-J., Ho, C., and Spiro, T. (1999) *J. Am. Chem. Soc. 121*, 11197−11203.
77. Dick, L. A., Heibel, G., Moore, E. G., and Spiro, T. G. (1999) *Biochemistry 38*, 6406−6410.
78. Juszczak, L. J., Manjula, B., Bonaventura, C., Acharya, S. A., and Friedman, J. M. (2002) *Biochemistry 41*, 376−385.
79. Jayaraman, V., Rodgers, K. R., Mukerji, I., and Spiro, T. G. (1995) *Science 269*, 1843−1848.
80. Blough, N. V., Zemel, H., and Hoffman, B. M. (1984) *Biochemistry 23*, 2883−2891.
81. Mozzarelli, A., Rivetti, C., Rossi, G. L., Eaton, W. A., and Henry, E. R. (1997) *Protein Sci. 6*, 484−489.
82. Bettati, S., Mozzarelli, A., Rossi, G. L., Tsuneshige, A., Yonetani, T., Eaton, W. A., and Henry, E. R. (1996) *Proteins 25*, 425−437.
83. Paoli, M., Liddington, R., Tame, J., Wilkinson, A., and Dodson, G. (1996) *J. Mol. Biol. 256*, 775−792.
84. Imai, K. (1982) *Allosteric effects in hemoglobin*, Cambridge University Press, Cambridge, England.
85. Shibayama, N., Morimoto, H., and Kitagawa, T. (1986) *J. Mol. Biol. 192*, 331−336.
86. Monod, J., Wyman, J., and Changeux, J. P. (1965) *J. Mol. Biol. 12*, 88−118.
87. Ackers, G. K. (1998) *Adv. Protein Chem. 51*, 185−253.
88. Ackers, G. K., Holt, J. M., Huang, Y., Grinkova, Y., Klinger, A. L., and Denisov, I. (2000) *Proteins (Suppl.)*, 23−43.
89. Friedman, J. M., Scott, T. W., Stepnoski, R. A., Ikeda-Saito, M., and Yonetani, T. (1983) *J. Biol. Chem. 258*, 10564−10572.
90. Shibayama, N., and Saigo, S. (2001) *FEBS Lett. 492*, 50−53.
91. Yonetani, T., Park, S., Tsuneshige, A., Imai, K., and Kanaori, K. (2002) *J. Biol. Chem. 37*, 34508−34520.
92. Miyazaki, G., Morimoto, H., Yun, K. M., Park, S. Y., Nakagawa, A., Minagawa, H., and Shibayama, N. (1999) *J. Mol. Biol. 292*, 1121−1136.
93. Ikeda-Saito, M., and Verzili, D. (1981) *J. Mol. Biol. 153*, 441−449.
94. Scott, T. W., Friedman, J. M., Ikeda-Saito, M., and Yonetani, T. (1983) *FEBS Lett. 158*, 68−72.

BI020648J